Novel insights on causes of disproportionate trends between particulate NO_3^- and NO_x emissions in Canadian urban atmospheres

Qinchu Fan[1], Xiaohong Yao[1,*], Leiming Zhang[2,*]

[1]Key Laboratory of Marine Environment and Ecology (MOE), and Frontiers Science Center for Deep Ocean Multispheres and Earth System, Sanya Oceanographic Institution, Ocean University of China, Qingdao 266100, China

[2]Air Quality Research Division, Science and Technology Branch, Environment and Climate Change Canada, Toronto, Ontario, M3H 5T4, Canada

* Corresponding author: Xiaohong Yao (xhyao@ouc.edu.cn), Leiming Zhang (leiming.zhang@ec.gc.ca)

Abstract. Particulate nitrate (NO_3^-) is a key target for air pollution control; however, its response to NO_x emission reductions remains uncertain, particularly in cold climates. This study assesses trends of fine- and coarse-mode NO_3^- (f-NO_3^- and c-NO_3^-) during 1990-2019 in seven Canadian cities, making use of the long-term data collected by the National Air Pollution Surveillance (NAPS) network, and revealed disproportionate trends between NO_3^- and NO_x emissions across Canada. In Edmonton, annual mean f-NO_3^- decreased by ~60% from 2007–2019 while provincial NO_x emissions declined by only 10–20%; comparable patterns were also observed in five out of the six other cities in the most recent decade. Such disproportionate trends were diagnosed to be caused by reduced primary f-NO_3^- emissions, localized dispersion, and Arctic Oscillation–modulated wind anomalies. Conversely, all cities exhibited a transient f-NO_3^- increase during 1998–2007, coincident with early NO_x controls and consistent with unintended enhancement of primary emissions of f-NO_3^- formed within stationary-combustion plumes. c-NO_3^- was largely insensitive to NO_x reduction in most cities (except Edmonton), with its trends governed by neutralization reactions with alkaline aerosols rather than HNO_3 availability. These findings help interpret the weak or absent response of f-NO_3^- to NO_x emission reductions observed worldwide, particularly in cold-climate regions.

Keywords: particulate nitrate, primary nitrate emission, decadal trends, NO_x emission reduction

1 Introduction

Particulate nitrate (NO_3^-) has been a central focus of pollution control strategies in the past several decades due to its impact on air quality, climate, and ecosystem health (Balamurugan et al., 2022; Dang et al., 2024; Thunis et al., 2021; Zhai et al., 2021; Bell et al., 2007; Chan et al., 2021; Cheng et al., 2024; Dabek-Zlotorzynska et al., 2011; Duce et al., 2008; Font et al., 2024; Harrison et al., 2022; Man et al., 2015; Pullokaran et al., 2024; Squizzato et al., 2018; Sun et al., 2025; Wang et al., 2020; Zaveri et al., 2021; Zhang et al., 2008; Zhou et al., 2022). NO_3^- impacts air quality because it is a major chemical component of particulate matter, particularly fine particles. Besides, photolysis of NO_3^- produces highly reactive oxidants, such as hydroxyl radicals, HOCl, and Cl_2, thereby enhancing atmospheric oxidation capacity (Chen et al., 2025; Gen et al., 2022; Peng et al., 2022). NO_3^- contributes to climatic effects directly through radiative forcing and indirectly through increasing cloud condensation nuclei (Drugé et al., 2019; Zaveri et al., 2021). For instance, a modeling study showed that nitrate aerosols contributed significantly to shortwave radiative cooling, reaching up to -5 W m^{-2} on a regional scale under clear-sky condition and -0.8 W m^{-2} on global average (Zaveri et al., 2021). NH_4NO_3 formed from condensation of gaseous species of NH_3 and HNO_3 can rapidly grow to the sizes of cloud condensation nuclei in cold atmospheres (Höpfner et al., 2019; Wang et al., 2022; Zhu et al., 2014). Additionally, NO_3^- contributes to atmospheric nitrogen deposition, which has ecosystem implications (Bose et al., 2018; Iizuka et al., 2025), and it can even undergo long-range transport in the atmosphere and eventually deposit into oceans or remote continental regions (Jonson et al., 2022; Qi et al., 2018; Iizuka et al., 2025).

Given the significant reductions of SO_2 emissions worldwide in the past four decades, the impacts of NO_3^- on air quality, climate, and ecosystem health have garnered increasing attention (Aas et al., 2019; Feng et al., 2020; Hand et al., 2024; Sun et al., 2018; Velazquez-Garcia et al., 2023; Wang et al., 2021; Zhai et al., 2021). Unlike

sulfate (SO_4^{2-}), which predominantly exists in fine particulate matter ($PM_{2.5}$), NO_3^- exists in both fine- and coarse-mode particles (referred to as f-NO_3^- and c-NO_3^-, respectively). As a semi-volatile substance, the fine and coarse fractions of NO_3^- vary with season and location (Peng et al., 2024; Yao and Zhang, 2012a, b; Zhang et al., 2008) because its volatility and partitioning with its gaseous precursors are influenced by ambient meteorological and chemical conditions, including temperature (T), relative humidity (RH), and mixing ratios of HNO_3 and NH_3 (Guo et al., 2016; Seinfeld and Pandis, 2016; Yao et al., 2003; Huo et al., 2025). This complicates the response of f-NO_3^- and c-NO_3^- to changes in NO_x emissions (Balamurugan et al., 2022; Chan et al., 2021; Thunis et al., 2021; Zhai et al., 2021; Huo et al., 2025). Additionally, reduced NO_x emissions may enhance the formation of N_2O_5 at nighttime, a product that can form f-NO_3^- through secondary aerosol formation, thereby further influencing the response of f-NO_3^- to emission reductions (Fan et al., 2020; Shah et al., 2018; Wang et al., 2023; Yan et al., 2023; Zhou et al., 2022; Ward et al., 2025). It has been reported that f-NO_3^- can form from condensable species in fresh stationary combustion plumes, followed by dispersion and evaporation under freezing ambient conditions (Shen et al., 2022; Xiao et al., 2025; Yang et al., 2024; USEPA, 2017). This mechanism ha been largely overlooked in studies examining the response of NO_3^- to NO_x emission reductions, particularly in regions with prolonged cold seasons.

Canada is a nation experiencing long cold winters. Higher concentrations of f-NO_3^- were predominantly observed during cold winter seasons, except during large-scale wildfire events mostly occurring in warm seasons (Bari and Kindzierski, 2016a, b; Dabek-Zlotorzynska et al., 2011; Edgerton et al., 2020; Jeong et al., 2011; Wang et al., 2021). The contributions of primary and/or secondary sources to the elevated f-NO_3^- concentrations in Canadian cold atmospheres remain poorly understood. The primary emissions of f-NO_3^- likely arise from two major processes: (i) the rapid formation of f-NO_3^- through reactions between HNO_{3gas} and NH_{3gas} within the first few seconds after combustion plumes exit the stack outlet (or vehicle exhaust pipes) and undergo cooling; and (ii) the formation of f-NO_3^- via the reaction $2NO_2 + H_2O \rightarrow HNO_3 + HNO_2$ within

droplets produced in fresh cooling combustion plumes, followed by NH_{3gas} neutralization before these droplets evaporate into ambient aerosols. Note that the fresh plumes contain extremely high concentrations of various air pollutants, enabling the occurrence of the above-mentioned reactions (Seinfeld and Pandis, 2016; Zhang et al., 2021; Zhang et al., 2023).

The aforementioned knowledge gap hinders our understanding of how changes in primary f-NO_3^- emissions influence the annual-scale response of f-NO_3^- to NO_x emission reductions. This gap appears to be global rather than unique to Canada, as indicated by the brief review of particulate NO_3^- trends and their responses to NO_x emission reductions summarized in Text S1 of the Supporting Information (SI). Two key points emerge. (1) The limited number of trend studies on particulate NO_3^- across Canada, including f-NO_3^- and total NO_3^- (=f-NO_3^-+c-NO_3^-) in suspended particles, suggest that long-term changes are neither spatially uniform nor monotonic. (2) The non-linear and sometimes counterintuitive response of particulate NO_3^- to NO_x emission controls has been widely reported in the United States, Europe, and China, yet the underlying drivers remain insufficiently constrained. Together, these cross-regional comparisons motivate a Canada-focused synthesis that explicitly evaluates the non-linear influences of co-evolving precursor emissions, gas–particle partitioning, and meteorological variability in interpreting long-term f-NO_3^- trends.

Additionally, significant decreases in NO_x emissions across Canada mainly occurred between 1998 and 2008, with slight time shifting across different provinces (ECCC, 2021). $PM_{2.5}$ speciation data since 2003 alone may not fully elucidate the response of NO_3^- to reduced NO_x emissions. Fortunately, both f-NO_3^- and c-NO_3^- data are available from the National Air Pollution Surveillance (NAPS) at 12 urban sites (Dabek-Zlotorzynska et al., 2019; Dabek-Zlotorzynska et al., 2011). Seven of these 12 sites have integrated measurements of particulate chemical components spanning 1-3 decades, enabling the examination of long-term trends in f-NO_3^- and c-NO_3^- in Canadian urban atmospheres and their responses to reduced NO_x emissions.

In this study we investigated long-term trends in the annual average mass concentrations of f-NO_3^- and c-NO_3^- in Canadian urban atmospheres, with a particular focus on the responses of f-NO_3^- and c-NO_3^- to NO_x emission reductions since 1990 and the associated mechanisms. The analyses are structured into three major parts: Part 1 examines the long-term trends of f-NO_3^- and c-NO_3^-, firstly in Edmonton (Section 3.1) and then extended the other six cities (Sections 3.2 and 3.3); Part 2 investigates the key factors influencing f-NO_3^- levels in Edmonton (Section 3.4) and the role of primary f-NO_3^- emissions in shaping these trends (Section 3.5); and Part 3 provides a comprehensive assessment of uncertainties associated with f-NO_3^- and their potential impact on the observed trends (Section 3.6). Finally, a summary of the major findings and potential implications are presented in Section 4.

2 Methodology

2.1 Monitoring sites and data sources

The present study utilized long-term data monitored at two urban sites in Edmonton (S-90132, Latitude: 53.486, Longitude: -113.465; and S-90130, Latitude: 53.544, Longitude: -113.499), as well as one urban site in each of the other six cities, including Winnipeg (49.898, -97.147), Victoria (48.442, -123.363), Vancouver (49.281, -122.849), Montreal (45.543, -75.572), Quebec City (46.821, -71.221), and Hamilton (45.258, -79.862) (Figures S1 and S2). The first four cities are in western Canada with Edmonton in the province of Alberta, Winnipeg in the province of Manitoba, and Victoria and Vancouver in the province of British Columbia. The other three cities are in eastern Canada with Montreal and Quebec City in the province of Quebec and Hamilton in the province of Ontario.

In Edmonton, at the S-90132 site speciation $PM_{2.5}$ samplers have been used since 2007 to measure mass concentrations of $PM_{2.5}$, ionic concentrations in $PM_{2.5}$, and the levels of acidic and alkaline gases, with 24-h integrated sampling occurring one in every three

days (Bari and Kindzierski, 2016a, b). At the S-90130 site, ionic species, including NO_3^-, SO_4^{2-}, NH_4^+, Na^+, and various elements in both $PM_{2.5}$ and $PM_{2.5-10}$ were collected using Dichotomous Air Samplers (Thermo, US), with 24-h integrated sampling occurring one in every six days during 1986-2005. Since no emission data were available before 1990, only the data after 1990 were included in this study. The ionic data were missing in 2006 at both sites. Note that the identical Dichotomous Air Samplers were also used at S-90132 for several years to collect $PM_{2.5}$, though no ionic data, for comparison purpose. Both datasets were included because neither alone covers the primary NO_x mitigation period in Edmonton.

In Hamilton, an identical speciation sampler has been used since 2013 to measure ionic components in $PM_{2.5}$ and gases, with sampling occurring one in every three days. In this city, only elements have been measured in samples collected by the Dichotomous Air Sampler since then. At the other five urban sites selected for this study, speciation $PM_{2.5}$ data were either unavailable (Winnipeg and Quebec City) or collected one in every six days after 2005 (Victoria, Vancouver, and Montreal). $PM_{2.5}$ air samplers (Thermo, US) were used in Victoria and Winnipeg after 2012, and $PM_{2.5}$ samplers (TISCH, US) were used in Vancouver and Montreal after 2016. Corresponding NO_3^- data in $PM_{2.5-10}$ were not available at these sites since then. In this study, NO_3^- in $PM_{2.5}$ collected by speciation samplers was also referred to as f-NO_3^-. The same definition is applied to f-SO_4^{2-} and f-NH_4^+, which were used to facilitate the analysis of f-NO_3^-.

Hourly average mass concentrations of $PM_{2.5}$ and mixing ratios of NO_2 were also routinely measured at each site, except that no NO_2 mixing ratios were reported at S-90132. In this case, the values from S-90130 were used in this study. For certain parts of the year at the sites in Victoria and Quebec City, NO_2 mixing ratios were also unavailable. In these cases, the mixing ratios of NO_2 measured at different sites within a 1-2 km radius in the same city were used to facilitate the analysis. All the data are publicly available through the National Air Pollution Surveillance (NAPS) program

network (https://data-donnees.ec.gc.ca/data/air/monitor/national-air-pollution-surveillance-naps-program/?lang=en) and summarized in Table S1.

NO_x, SO_2, and NH_3 emissions data at the provincial level in Canada were obtained from https://www.canada.ca/en/environment-climate-change/services/environmental-indicators/air-pollutant-emissions.html. The monthly average wind fields were downloaded from https://psl.noaa.gov/data/gridded/data.narr.html (Figures 1 and S1), and the Arctic Oscillation (AO) Indexes were obtained from https://www.ncdc.noaa.gov/teleconnections/ao/ (Figure S1d). Ground-level meteorological data from the airports of these cities were also downloaded from https://www.wunderground.com/about/data.

It should be noted that existing techniques for measuring ambient HNO_{3gas} are subject to certain artifacts. Specifically, the Na_2CO_3-coated denuder used in speciation samplers is designed to remove acidic gases upstream of $PM_{2.5}$ collection on a Teflon filter, thereby minimizing positive artifacts in the collected $PM_{2.5}$ (Dabek-Zlotorzynska et al., 2019; Dabek-Zlotorzynska et al., 2011). However, measurements obtained using the denuder technique do not exclusively represent HNO_{3gas}. Instead, they include HNO_{3gas}, N_2O_{5gas}, and other acidic gases that react with Na_2CO_3 to form $NaNO_3$. Consequently, the reported concentrations reflect an upper bound of (HNO_{3gas} + N_2O_{5gas}). To avoid ambiguity, the measured values are denoted as HNO_{3gas}* rather than HNO_{3gas} throughout the following discussion. Importantly, this measurement uncertainty does not materially affect the conclusions of the present study, as HNO_{3gas}* concentrations remain substantially lower than the corresponding particulate nitrate levels during the high-nitrate winter periods examined here (see Section 3.4). Nevertheless, the upper-bound nature of HNO_{3gas}* may introduce bias in gas–particle equilibrium analyses, particularly during winter nighttime high-concentration episodes, when the true HNO_{3gas} mixing ratio may be considerably lower than HNO_{3gas}* due to a potentially substantial contribution from N_2O_5(g).

2.2 Statistical analysis

Annual average mass concentrations of f-NO_3^- and c-NO_3^- were calculated from all available data in each calendar year. However, data loss was common in each city and year despite sampling occurring one in every three or six days. To minimize uncertainty from data loss and ensure sufficient data for trend analysis, data for trend analysis were excluded for any year when measurements for two consecutive months were unavailable. To analyze the time series of the annual average mass concentrations of each species, the Mann-Kendall (M-K) analysis was employed. The qualitative trend results determined by the M-K method include: (i) an increasing/decreasing trend with a *P* value of <0.05, (ii) a probable increasing/decreasing trend with a *P* value between 0.05 and 0.1, (iii) a stable trend with a *P* value >0.1, as well as a ratio of <1.0 between the standard deviation and the mean of the dataset, and (iv) a no trend with a *P* >0.1 and other conditions (Lin et al., 2022).

To quantify the overall effect of climate anomalies on the annual average f-NO_3^- between a pair of two years, our recently developed identical-percentile regression analysis was used (Lin et al., 2022; Yao and Zhang, 2024). In this method, the data sizes of the paired two-year should be the same (e.g., with the same time resolution and filling up all the missing data). The two sets of data, originally in time series, are sorted separately from the smallest to the largest to generate two percentile-based data arrays, which were then used for regression analysis with the intercept being set to be zero. The regression analysis can also be conducted using data in any particular percentile range for exploring different research targets. If the data sizes of the paired two-year are different, the one with a larger size can be modified to match the one with a smaller size using the method presented by Lin et al. (2022) and Yao and Zhang (2024) before applying the regression analysis described above. Moreover, a Random Forest (RF) model was employed to evaluate the relative importance of meteorological and seasonal timing variables in driving f-NO_3^- formation (Text S2 of SI), and the Flexible 0-D

Atmospheric Model (F0AM) was applied to simulate secondary production of f-NO_3^- (Text S3 of SI).

3 Results and discussion

3.1 Complexity of particulate nitrate trends in urban atmosphere of Edmonton

As mentioned in Section 2.1, two sites (S-90130 and S-90132) in Edmonton were selected for investigation due to the discontinued data coverage at both sites. Annual average mass concentrations of f-NO_3^- at S-90130 from 1990 to 2005 and at S-90132 from 2007 to 2019 were analyzed to illustrate the complexity of particulate nitrate trends in the urban atmosphere (Figure 1a). As mentioned in Section 2.1, data in 2006 were missing at both sites. For comparison, annual average mass concentrations of c-NO_3^- at S-90130 from 1990 to 2005 are also shown in Figure 1a and those of f-NH_4^+ and f-SO_4^{2-} at S-90130 and S-90132 from 1990 to 2019 are shown in Figure S3. To facilitate analysis, annual average mixing ratios of NO_2 at S-90130 from 1995 to 2019 are shown in Figure 1b, and annual provincial total emissions of NO_x, SO_2, and NH_3 in Alberta are also presented (Figures 1b, S3a and S3c, respectively). Correlation analyses between f-NO_3^- (or c-NO_3^-) and provincial total emissions of NO_x in 1990-2005 and between f-SO_4^{2-} and provincial total emissions of SO_2 in 1990-2019 are conducted (Figures 1c and S3b, respectively).

At S-90130, annual average f-NO_3^- and c-NO_3^- was 0.48 ± 0.25 μg m^{-3} (average ± standard deviation) and 0.15 ± 0.05 μg m^{-3}, respectively, during 1990 - 2005. No trend or stable trend was found for these species ($P > 0.10$), likely due to a bell-shaped change in provincial total NO_x emissions from 1990 to 2005. In fact, a significant correlation was found between annual average c-NO_3^- and provincial total NO_x emissions during 1990-2005 ($P < 0.01$). However, a significant correlation between annual average f-NO_3^- and provincial NO_x emissions was obtained only during 1992-2005 ($P < 0.01$), but not for the entire period during 1990-2005 with the values in 1990-1991 being substantially deviating from the regression curve. Such a deviation is yet to be

explained. Notably, f-NO_3^- and c-NO_3^- were not significantly correlated in any individual year during 1990–2005 ($R^2 < 0.1$; $P > 0.05$). The same pattern was observed at the other six sites analyzed in this study. The lack of correlation between f-NO_3^- and c-NO_3^- is discussed in detail in Section 3.2.

At S-90132, annual average f-NO_3^- was 1.3 ± 0.40 μg m^{-3} during 2007 - 2019. f-NO_3^- exhibited a decreasing trend ($P < 0.01$), with a Sen's Slope of 0.063 μg m^{-3} yr^{-1}, resulting in an overall decrease of approximately 60% during this period. In comparison, the monitored NO_2 mixing ratios at a different site (S-90130) decreased by approximately 20%, while provincial total NO_x emissions in Alberta were reduced by only ~10% during the same period. Such disproportionate decreases were also identified for both f-NO_3^- and c-NO_3 at S-90130 in the selected period of 1997-2005, with a ~60% decrease in their annual average concentrations compared to a ~20% decrease in both the NO_2 mixing ratios and provincial NO_x total emissions. Notably, NO_2 mixing ratios at the urban site were significantly correlated with Alberta's total provincial NO_x emissions, with $R^2 = 0.81$ over 1997–2019 ($P < 0.01$) and a slightly weaker correlation ($R^2 = 0.57$) over the shorter period of 2007–2019 ($P < 0.01$). These results indicate broadly consistent NO_x mitigation signals at both the provincial and city scales. Thus, the disproportionate large decrease in the annual average f-NO_3^- at S-90132 relative to the reduction in provincial NO_x emissions is analyzed below by considering major driving factors (Section 3.4), primary and secondary sources (Section 3.5), and potential uncertainties in the data of the generated annual average f-NO_3^- (Sections 3.6). It should be noted that the annual average f-NO_3^- measured at S-90132 in 2007-2019 were significantly higher than those recorded at S-90130 in 1990-2005 ($P<0.01$), which could be attributed to an unexpected mitigation effect, as analyzed in Section 3.3 below.

Unlike f-NO_3^-, annual average f-SO_4^{2-} exhibited a relatively smooth decreasing trend ($P < 0.01$), with a Sen's slope of 0.029 μg m^{-3} yr^{-1} if combining data at S-90130 from 1990 to 2005 and at S-90132 from 2007 to 2019 together (Figure S3a). This trend was

mostly consistent with a 0.021 μg m^{-3} yr^{-1} decrease in the provincial total SO_2 emissions from 1990 to 2019. Additionally, a moderately strong correlation was found between the annual average f-SO_4^{2-} and the provincial total SO_2 emissions over the three decades ($P < 0.01$, Figure S3b). The f-SO_4^{2-} trend in the urban atmosphere reflects the mitigation effect, as has also been reported for rural atmospheres in Canada (Cheng and Zhang, 2017; Feng et al., 2020). f-SO_4^{2-}, typically formed through in-cloud aqueous reactions and with non-volatile properties, is generally associated with regional sources, and thus tends to be spatially homogeneously distributed in urban scales (Bell et al., 2007; He et al., 2001; Park et al., 2004). This may explain the much smaller gaps in the annual average f-SO_4^{2-} between the two nearby urban sites, as compared to the case of f-NO_3^- .

Annual average f-NH_4^+ exhibited a decreasing trend ($P < 0.05$) if combining data at S-90130 from 1990 to 2005 and at S-90132 from 2007 to 2019 (Figure S3c). However, the trend was stable at both sites during the two separate periods ($P > 0.10$). From 1990 to 2019, the provincial total NH_3 emissions increased by approximately 40% (Figure S3c). The phenomenon of the decoupled trends between f-NH_4^+ and NH_3 emissions widely occurred in Canada and the U.S. in the recent decades, as reported in Yao and Zhang (2019). This is because the level of f-NH_4^+ was mainly controlled by those of SO_4^{2-} and NO_3^- through neutralization reactions, especially under NH_3-rich conditions (Bari and Kindzierski, 2016b; Dabek-Zlotorzynska et al., 2011; Edgerton et al., 2020). The equivalent ratios of NH_4^+ to (SO_4^{2-} + NO_3^-) in two selected years support this hypothesis (Figure S4).

3.2 Trends of f-NO_3^- and c-NO_3^- in urban atmospheres of Winnipeg – an inland city in western Canada

The annual average f-NO_3^- in Winnipeg varied within a range of 0.07-0.70 μg m^{-3}, with a long-term average of 0.32 ± 0.15 μg m^{-3} from 1990 to 2018. A stable trend in annual average f-NO_3^- was identified by the M-K method ($P = 0.51$; Figure 1d). The annual average c-NO_3^- varied within an even smaller range of 0.13-0.29 μg m^{-3}, with a long-

311 term average of 0.19 ± 0.04 μg m^{-3} during 1990–2012. A probable increasing trend in
312 annual average c-NO_3^- was identified (P = 0.06). Over the same period, both the annual
313 average mixing ratio of NO_2 at this site and provincial total NO_x emissions in Manitoba
314 exhibited decreasing trends (P < 0.01) (Figure 1e), and they correlated with each other
315 strongly (R^2 = 0.90, P < 0.01). The absence of a corresponding decrease in f-NO_3^-
316 concentration compared to NO_x emissions is likely attributable to enhanced primary
317 emissions of f-NO_3^--containing aerosols, as discussed in Sections 3.3 and 3.5 below.
318 This is clearly supported by the following evidence: from 1999 to 2004, annual average
319 f-NO_3^- increased by approximately 200%, even as provincial NO_x emissions and NO_2
320 mixing ratios declined by about 10%. Accordingly, the trend in f-NO_3^- concentrations
321 was analyzed in two separate periods: 1990–2002 and 2003–2018. The year of 2003 is
322 allocated into the second rather than the first period based on the curve of annual
323 variation shown in Figure 1d. In the first period (1990–2002), f-NO_3^- showed a probable
324 decreasing trend, with a Sen's Slope of 0.017 μg m^{-3} $year^{-1}$ and a total decline of about
325 80%. This sharp decrease cannot be explained by the relatively modest 10–20%
326 reductions in NO_2 and NO_x during the same period, suggesting that highly localized
327 factors and/or uncertainties caused by coarse resolution data (1 in every 6 days) were
328 likely the dominant contributors. The related uncertainty analysis is presented in
329 Section 3.6 below. In the second period (2003–2018), f-NO_3^- exhibited a decreasing
330 trend with a Sen's Slope of 0.018 μg m^{-3} $year^{-1}$, amounting to an overall reduction of
331 approximately 70%, which also exceeded the ~50% reduction in NO_2 mixing ratios at
332 the same site and the ~30% reduction in provincial NO_x emissions. The
333 disproportionate trends between f-NO_3^- and NO_x emissions observed in Winnipeg are
334 similar to the case in Edmonton discussed above.
335
336 When the time series of daily concentrations of f-NO_3^- and c-NO_3^- were examined for
337 a low-concentration year (1996) and a high-concentration year (2007) (Figure 1f-g),
338 elevated concentrations of f-NO_3^- were predominantly observed during the cold
339 months. High concentrations of f-NO_3^- were likely from primary sources, as discussed
340 in Section 3.5 below, considering the similar climate in inland western Canada. This,

however, needs to be confirmed using HNO_{3gas}^* data, which are not available at this site. In contrast, elevated concentrations of c-NO_3^- typically occurred during warmer months. Again, no significant correlation was observed between f-NO_3^- and c-NO_3^- in any year (R^2<0.1, P>0.05). Given the probable increasing trend in annual average c-NO_3^- despite decreasing NO_x emissions at both city and provincial scales, and considering the seasonal pattern of elevated levels, it is likely that the trend in c-NO_3^- was governed by the availability of alkali aerosols associated with suspended road dust and road-salt particles capable of neutralizing HNO_{3gas}^*, rather than by changes in HNO_{3gas}^* itself. As further illustrated in Section 3.4 below for the case of Edmonton, stagnant winter meteorological conditions did not coincide with elevated HNO_{3gas}^* concentrations, likely due to the accompanying sub-freezing temperatures. Moreover, stagnant and freezing conditions are not conducive to the suspension of road dust and road-salt particles during winter. This interpretation is also supported by findings reported in literature at rural sites in Canada (Cheng and Zhang, 2017; Feng et al., 2020) and urban and rural sites in the U.S. (Sickles II and Shadwick, 2015) and U.K. (Tang et al., 2018), where positive correlations between HNO_{3gas}* and NO_2 have been observed, suggesting that a reduction in NO_x would not typically lead to enhanced HNO_{3gas}^* formation.

3.3 Time window for unintended effects of NO_x mitigation on f-NO_3^- aerosols in Canadian urban atmospheres and associated shaped trends of f-NO_3^- and c-NO_3^-

Long-term trends of f-NO_3^- could be distorted by unintentionally increased f-NO_3^- primary emissions resulted from certain NO_x mitigation measures. Such phenomena were repeatedly observed in urban atmospheres across Canada during a consistent time window from approximately 1998 to 2007, as illustrated in Figures 1, and S5 as well as those aforementioned in Edmonton and Winnipeg. During this period, similar NO_x mitigation actions were taken in both Canada and the U.S., regulated by the Canada - U.S. Air Quality Agreement signed in 1991and further expanded in 2000. Although mitigation policies were likely implemented independently in each province in Canada, and the exact timing may have varied slightly, a consistent pattern emerged. For

example, in the province of Quebec, the annual average f-NO_3^- increased by approximately 150% in Quebec City from 1998 to 2003 and by around 300% in Montreal from 1998 to 2002. During the same period, annual average mixing ratio of NO_2 decreased by approximately 10% in both cities, while provincial total NO_x emissions remained nearly unchanged. In the province of Ontario, annual average f-NO_3^- in Hamilton remained relatively low at 0.69 ± 0.09 μg m^{-3} during 1995–1999, but rose sharply to 1.6 μg m^{-3} in 2001, with a notable dip to 0.85 μg m^{-3} in 2002 possibly due to climate anomaly, bounced back to 1.7 μg m^{-3} in 2004 and stabilized at 1.6 μg m^{-3} in 2005. During the period from 1999 - 2005, both observed NO_2 mixing ratios in Hamilton and provincial NO_x emissions in Ontario began to decline by 20–30%. A similar pattern was also found in western coastal urban areas such as Victoria and Vancouver, both located in British Columbia, between 1998 and 2002 (Figure 2), where annual average f-NO_3^- increased by approximately 100% while NO_2 mixing ratios and provincial NO_x emissions declined by 10–30%. These widespread, disproportionate trends between f-NO_3^- and NO_x emissions across multiple cities strongly suggest that, during this early control window, NO_x mitigation measures may have been accompanied by an unintended increase in primary f-NO_3^- emissions, potentially associated with condensable particulate matter (CPM) and/or byproducts of emission control technologies. However, no direct facility measurement data were made 20-year ago to verify this hypothesis. In fact, the USEPA only issued the method protocol for determining condensable particulate matter in 2017. Evidence from recent studies in developing countries further indicates that early-stage NO_x controls (e.g., NH_3-SCR operated at >300 °C) can be susceptible to imperfect ammonia dosing and the formation of associated byproducts (Yang et al., 2016). This provides a plausible mechanistic explanation, although the specific causes in Canada and the United States cannot be definitively determined in the absence of historical CPM measurements. Accordingly, trend analysis of particulate nitrate should treat this period separately, with a demarcation line drawn at approximately 2002 or later.

In contrast to this early-phase behavior, several lines of evidence suggest that primary f-NO_3^- emissions have likely declined in recent years. At the national scale, Canada's electricity supply has shifted markedly toward CO_2-emission-free sources (now exceeding 80%), which are also largely free of NO_x emissions. This transition should reduce primary nitrate-related emissions from the power sector (Canada Electricity Advisory Council, 2024). In addition, the rapidly increasing share of zero-emission vehicles, accounting for 10.8% of new vehicle registrations in 2023, is expected to further decrease primary f-NO_3^- emissions from the transportation sector (Statistics Canada, 2024). Consistent with these broader trends, observations in Edmonton show that the decline in annual mean f-NO_3^- concentrations over the past decade has been substantially larger than the corresponding decrease in NO_2. This divergence supports the interpretation that reductions in primary f-NO_3^- emissions have likely been an important contributing factor.

Setting the demarcation line at 2003 in Quebec City (noting the substantial data loss in 2002 for this city) and at 2002 in Montreal, the annual average f-NO_3^- decreased by more than 70% over the subsequent 16- or 17-year period, largely agree with the 40-60% reductions in NO_2 mixing ratios and provincial NO_x emissions during the same period. The slight differences in their decreasing rates could be attributed to unintended changes in primary emissions of f-NO_3 aerosols as discussed above, non-linear atmospheric chemistry process involving other chemical species, and data uncertainties, etc. Notably, the annual average c-NO_3^- showed no significant trend during these periods in either city, suggesting that c-NO_3^- levels may have been more strongly influenced by the presence of alkali aerosols capable of neutralizing HNO_{3gas}^* rather than by the availability of HNO_{3gas}^* itself. Data prior to 2002 (Montreal) or 2003 (Quebec City) were insufficient in duration to support robust trend analysis; nevertheless, the influence of unintended mitigation effects during this period was still evident. In comparison, if removing the demarcation line and considering the whole data record together, annual average f-NO_3^- would show no clear trend from 1995 to 2018 in Quebec City and a stable trend from 1997 to 2018 in Montreal. Over the full

period, annual average f-NO_3^- and c-NO_3^- were 0.41 ± 0.19 μg m^{-3} and 0.19 ± 0.05 μg m^{-3}, respectively, in Quebec City and 0.57 ± 0.38 μg m^{-3} and 0.28 ± 0.06 μg m^{-3}, respectively, in Montreal.

Similarly, if setting a demarcation line at the year of 2002 for Victoria and Vancouver, f-NO_3^- would show either a significant decreasing trend or a probable decreasing trend, with a total decrease of around 40% in both cities from 2002 to 2018. These declines were broadly consistent with the 30–40% decreases in both NO_2 mixing ratios and provincial NO_x emissions during the same period. From 1990 to 2002, f-NO_3^- showed either no trend or a stable trend, which was consistent with the trend in the provincial NO_x emissions, but inconsistent with the observed decreasing trend in NO_2 mixing ratio during this period. If looking at the full data record of c-NO_3^- together (from 1990 to 2012 in Victoria or 2015 in Vancouver), either no trend or a stable trend was identified in either city, regardless of using the full data record or just data after the year 2002. The absence of a clear decreasing trend in c-NO_3^- concentration, despite significant NO_x emissions, appears to be a common feature across Canadian urban environments. Unlike the other cities aforementioned where annual average concentrations of f-NO_3^- were much higher than those of c-NO_3^-, in Victoria, annual average concentrations of f-NO_3^- and c-NO_3^- were similar, oscillating around 0.23 ± 0.06 μg m^{-3} (1990 to 2018) and 0.25 ± 0.05 μg m^{-3} (1990 to 2012), respectively. In contrast, annual average concentrations of f-NO_3^- (0.16 ± 0.05 μg m^{-3} in 1990 - 2018) were significantly smaller than that of c-NO_3^- (0.31 ± 0.05 μg m^{-3} in 1990 - 2015) (P<0.01) in Vancouver, and the same conclusion can be generated if only using data in 1990-2015.

In Hamilton, no statistically significant trends were identified for f-NO_3^- and c-NO_3^-, whether considering the full time series or just the period post-2005. This is somewhat different than the cases in the other cities discussed above, suggesting potentially strong impact of local sources, besides the other main factors discussed above, considering that Hamilton is an industrial city with heavy density of industries. Annual average f-

NO_3^- and c-NO_3^- in this city were 0.88 ± 0.35 μg m^{-3} and 0.46 ± 0.12 μg m^{-3}, respectively, during the period of 1995 to 2019.

3.4 Key factors influencing annual average f-NO_3^- and its trends in Edmonton

To explore key factors influencing the annual average f-NO_3^- and its trends in Edmonton, we selected data from two representative years (2010 and 2015) at site S-90132 for comparative analysis. The year 2010 was chosen because in this year abnormally high annual average f-NO_3^- was observed compared to all the other years during the period of 2007-2019, suggesting possible impact by climate anomaly in this year. The year 2015 was chosen because in this year annual average f-NO_3^- represents the median value of a five-year period of 2015-2019, likely reflecting the average climatic conditions, knowing that the annual average NO_2 mixing ratio observed at a nearby site (S-90130) and the provincial total NO_x emissions were nearly constant during 2015-2019. From 2010 to 2015, the decrease in NO_2 mixing ratios in Edmonton (11%) was consistent with the decline in Alberta's provincial NO_x emissions (10%). In contrast, the annual mean concentration of f-NO_3^- decreased much more sharply (by 58%), falling from 2.1 μg m^{-3} in 2010 to 0.89 μg m^{-3} in 2015.

Through the comparative analysis, seasonal variations of f-NO_3^-, various single-factor effects on f-NO_3^-, and the impact of climate anomalies on f-NO_3^- were explored. As shown in Figures 3a and 3b, higher concentrations of f-NO_3^- were predominantly observed during cold months, including January to March and November to December, in both 2010 and 2015. These higher concentrations during the five cold months contributed to 81% and 88% of the annual averages in 2015 and 2010, respectively. Thus, the annual trends in f-NO_3^- were mainly determined by higher concentrations of f-NO_3^- in cold months in Edmonton. Based on wind fields shown in Figures S1 and S2, air masses reaching to this site in the cold winter should come from the remote northern areas with low pollution levels due to the strong northwest wind, which should have lowered concentrations of f-NO_3^- in the urban atmosphere. Thus, the high concentrations of f-NO_3^- observed at this site should be caused by local accumulation

under stagnant weather conditions. Therefore, the emissions of f-NO_3^--contained aerosols related to mitigation measures, the precursors and formation pathways of f-NO_3^-, and meteorological conditions during the winter period should be considered as key factors determining the annual average f-NO_3^-.

We then correlated the 24-hr integrated daily concentrations of f-NO_3^- with ambient T, wind speed (WS), RH, and gaseous HNO_3 (HNO_{3gas}) to explore various single-factor effects on f-NO_3^- (Figure 3). A demarcation line was observed at -3°C in 2010 and 0.5°C in 2015, with substantially lower f-NO_3^- concentration at T on the right than left side of the line (Figures 3a and 3e). Lower ambient T favored the gas-aerosol partitioning of NH_4NO_3 in $PM_{2.5}$ (Seinfeld and Pandis, 2016; Shah et al., 2018). However, lower ambient T also weakened photochemical reactions due to reduced amounts of intermediate volatility organic compounds or semi-volatile organic compounds in the gas phase (McDonald et al., 2018; Wernis et al., 2022). This reduction in photochemical activity subsequently lowered the concentration of HNO_{3gas} to some extent, e.g., the concentrations of HNO_{3gas} observed at T > 20°C increased by over a factor of four relative to those at T < -10°C in 2015 as shown in Figures 3e. The sources of f-NO_3^- and its formation pathways during the winter period will be revisited in Section 3.5. The causes for the different T values of the demarcation line between 2010 and 2015 are not clear. The concentrations of f-NO_3^- decreased with increasing WS due to the dispersion effect, and no elevated concentrations were observed once WS is stronger than 5 m/s (Figures 3b and 3f). The concentrations of f-NO_3^- had little dependence on ambient RH (Figure 3c and 3g), e.g., the highest concentrations in both years occurred at RH of 70-80% instead of >80%. The lowest concentrations of f-NO_3^- appearing at RH < 60% is because RH < 60% typically occurred at ambient T greater than 0°C in Edmonton. In addition, the relative importance of 15 major variables on f-NO_3^- concentration was examined using a Random Forest model, as detailed in Text S2 of SI. The ambient T ranked as the dominant factor, followed by $PM_{2.5}$ mass concentration, NO_2 mixing ratio, boundary layer height, etc.

It should be noted that gas–particle equilibrium between HNO_3–NH_3 and submicron NH_4NO_3 is unlikely to be achieved at temperatures below -10 °C, given the relatively long equilibration timescales. Based on the results of characteristic timescales analysed by Wexler and Seinfeld (1990, 1992) and dynamically simulated by Meng and Seinfeld (1996), particles with diameters of approximately 0.5–0.7 μm generally require hours to approach equilibrium – typically on the order of ~1–6 h with a more conservative upper bound of ~6–20 h. Under such low-temperature conditions, the assumption of instantaneous thermodynamic equilibrium becomes questionable; therefore, equilibrium thermodynamic modelling was not applied here. At even lower temperatures, the equilibration timescale would extend to tens of hours for highly viscous or glassy particles, as suggested by Li and Shiraiwa (2019).

Correlation analysis between simultaneously measured f-NO_3^- and HNO_{3gas}^* showed that f-NO_3^- concentrations higher than 4 μg m^{-3} occurred when HNO_{3gas}^* concentrations were lower than 0.4 μg m^{-3} in both years (Figures 3d and 3h). Thus, the high f-NO_3 concentrations were not likely caused from the secondary formation of f-NO_3^- from HNO_{3gas}^* in ambient air, as further discussed in Section 3.5 below. Considering that the concentrations of NH_{3gas} (data not shown here) were generally more than one order of magnitude higher than those of HNO_{3gas}^*, NH_{3gas} should not be the limiting factor for f-NO_3^- formation, and was therefore excluded from further analysis below.

Climate anomaly can have significant impacts on air pollution (Andersson et al., 2007; Wetherbee and Mast, 2016; Yao and Zhang, 2020). One of the factors related to climate anomaly in winter Canadian urban atmospheres is AO (Yao and Zhang, 2020; Burakowski et al., 2008; Higgins et al., 2002). Other climate drivers, such as ENSO, Arctic sea-ice variability, and long-term warming, may influence f-NO_3^- during the warming season. However, their impact on the annual trend is likely negligible, as it is dominated by wintertime f-NO_3^-. As shown in Figures S1 and S2, the mean wind speed from January to March across Alberta decreased significantly in 2010 compared to the other years. The AO index during the winter period in 2010 was in the most negative

phase observed in the last four decades (Figure S1d). Typically, the belt of strong winds circulating around 55°N latitude weakens during such a phase, which allows colder Arctic air masses to penetrate further south into the mid-latitudes (Higgins et al., 2002). The substantial decrease in WS during the winter period of 2010 likely contributed to the higher annual average f-NO_3^- in this year. It is noticed that the recorded ambient T in Edmonton in this winter was similar to the climatic mean value (https://www.wunderground.com/about/data), further supporting the hypothesis that it is the weaken WS caused by AO anomaly, rather than changes in T, that enhanced the accumulation of f-NO_3^-.

To further examine the effects of the AO anomaly on f-NO_3^- accumulation in 2010 relative to that in 2015, we conducted the identical-percentile regression analysis between the two years (Figures 4c-e). With the intercept being forced to zero, similar to the approach commonly used in chemical experiments for establishing the standard curve (Yao et al., 2011), the slope of the regression equation was 2.74 if using all the data (0^{th} to 100^{th} percentiles), 1.56 if using the central 50% data (25^{th} to 75^{th} percentiles), and 1.41 if only using the lower 50% data (0^{th} to 50^{th} percentiles). The differences in f-NO_3^- concentration between the two years were clearly enlarged when higher concentrations were included, due to the AO anomaly effect in the winter of 2010. Assuming a log-normal distribution of the data, the lower percentiles and higher percentiles data, i.e., 0^{th} to 2.5^{th} percentiles and 97.5^{th} to 100^{th} percentiles, are normally excluded from 95% confidence level. This is because these data points have lower probability densities and their corresponding values are more vulnerable to climate anomaly impact such as AO with negative and positive phases. The highest probability density should always occur at the 50^{th} percentile, where the corresponding value should be least affected by AO. To minimize potential error from using a single value, we used the average values of the 47.5^{th}-52.5^{th} percentiles, which were 0.63 μg m^{-3} in 2010 and 0.45 μg m^{-3} in 2015. The ratio of these two values (=1.4) was nearly identical to the slope of the regression equation using data from the 0^{th} to 50^{th} percentiles presented above. Thus, the annual average f-NO_3^- in 2010 was recalculated by the

corresponding value in 2015 being multiplying by a factor of 1.4 in order to deduct the AO anomaly effect. The recalculated annual average f-NO_3^- in 2010 would decrease from the original value of 2.1 μg m^{-3} to 1.2 μg m^{-3}. Interestingly, removing the AO effect in 2010 would only have a minor impact on the decadal trends from 2007 to 2019, e.g., the Sen's Slope only showed small changes: which was 0.063 μg m^{-3} $year^{-1}$ using the original annual average values including the year 2010, 0.060 μg m^{-3} $year^{-1}$ if excluding the year 2010, and 0.057 μg m^{-3} $year^{-1}$ if replacing the year 2010 value with 1.2 μg m^{-3}.

Overall, the AO largely affected the annual average f-NO_3^- in 2010. Nevertheless, such an impact only has marginal effects on the decadal trends of f-NO_3^-, as the AO typically oscillates between negative and positive phases within 2-3 years (Figure S1d). The enhanced or weakened effects of AO in 2-3 years can be largely canceled out in extracting the decadal trend of f-NO_3^-. The overall effect appeared to be too small to explain the above-mentioned disproportionate responses of the annual average f-NO_3^- to the reduced NO_x emissions, and more exploration on this issue is presented in Sections 3.5 and 3.6 below.

3.5 Rethinking the role of primary emissions of NH_4NO_3 during the cold season in Canadian urban atmospheres

From the analysis presented in the previous section we concluded that the high concentrations of f-NO_3^- in the winter were mainly due to local accumulation under stagnant meteorological conditions, rather than long-range transport driven by northwesterly winds. This raised the fundamental question: what is the role of primary emissions in combustion plumes or secondary formation of NH_4NO_3 in ambient air in contributing to f-NO_3^- in Canadian urban atmospheres during the cold season? To answer this question, we proposed a hypothesis, i.e., whether HNO_{3gas*} concentrations significantly increased under conditions with low f-NO_3^- concentrations compared to cases with high f-NO_3^- concentrations, and then examined the hypothesis below.

606 Theoretical analysis and implications of the hypothesis were provided in supplementary
607 information (Text S3 of SI).
608
609 To examine the weaker hypothesis outlined above, we first divided the 2010
610 observations into two temperature regimes: $T < 0°C$ and $0°C < T \leq 4°C$. Observations
611 with $T < 0°C$ were further divided into two subsets based on f-NO_3^- concentrations,
612 using the thresholds of > 4 μg m^{-3} and ≤ 4 μg m^{-3}. These three groups were then
613 compared, i.e., Group 1: $T < 0°C$ and f-NO_3^- > 4 μg m^{-3}, in which case there were 19
614 samples with average HNO_{3gas}^* and f-NO_3^- concentrations being 0.15 ± 0.09 μg m^{-3} and
615 8.8 ± 4.4 μg m^{-3}, respectively; Group 2: $T < 0°C$ and f-NO_3^- < 4 μg m^{-3}, in which case
616 there were 26 samples with average HNO_{3gas}^* and f-NO_3^- concentrations being $0.15 \pm$
617 0.12 μg m^{-3} and 1.3 ± 0.7 μg m^{-3}, respectively; and Group 3: $0°C < T \leq 4°C$, in which
618 case there were 13 samples with average HNO_{3gas}^* and f-NO_3^- concentrations being
619 0.15 ± 0.11 μg m^{-3} and 1.3 ± 1.7 μg m^{-3}, respectively. Apparently, the average HNO_{3gas}^*
620 concentrations did not differ between the three Groups ($P < 0.01$); thus, the initial
621 hypothesis has to be rejected. This suggests that the process of secondary formation of
622 NH_4NO_3 from HNO_{3gas}^* was not the main contributor to the observed high
623 concentrations of f-NO_3^-, leaving the process of primary emissions as the only major
624 contributor. In addition, the markedly reduced f-NO_3^- concentrations at $T > 0°C$ were
625 likely due to volatilization of a portion of primarily emitted f-NO_3^-.
626
627 To further test the robustness of the above analysis, we expanded the dataset to include
628 measurements at $T \leq 4°$ from both 2010 and 2015, yielding a total of 108 f-NO_3^-
629 samples (Group 1: n = 23; Group 2: n = 54; Group 3: n = 31). The mean (± SD)
630 concentrations of f-NO_3^- and HNO_{3gas*} were 8.7 ± 4.1 μg m^{-3} and 0.16 ± 0.11 μg m^{-3}
631 for Group 1, 1.4 ± 0.95 μg m^{-3} and 0.17 ± 0.16 μg m^{-3} for Group 2, and 0.9 ± 1.1 μg m^{-3} and 0.15 ± 0.10 μg m^{-3} for Group 3, respectively. Even with the expanded dataset,
633 mean HNO_{3gas*} did not differ significantly among the three groups (Welch one-way
634 ANOVA, $p = 0.74$), despite the intentionally large contrast in f-NO_3^- imposed by the
635 group definitions.

The above analysis results suggest that the trend of f-NO_3^- in Edmonton was likely governed by the primary emissions of f-NO_3^- aerosols, as well as the extents of their volatilization and dispersion during the cold season. The dependence of volatilization of f-NO_3^- on ambient T and dispersion on WS has been recently confirmed in observational and modeling studies (Huo et al., 2025; Peng et al., 2024; Shen et al., 2022). As mentioned in the Introduction, the primary emissions of f-NO_3^- likely have two major sources (or processes). The first source is also conventionally defined as condensable particulate emission and associated with the combustion of (N_2 + O_2), which produces various oxidized nitrogen species, including HNO_{3gas}^*, NO_x, etc. (USEPA, 2017). The amount of primary NH_4NO_3 formed from HNO_{3gas*} in cooling plumes theoretically depends on the combustion technology, the use of catalytic reduction systems employing NH_3, and the ambient T (Zhang et al., 2021; Tayyeb Javed et al., 2007; Palash et al., 2013), which may not be controlled by NO_x emission levels. In some reported cases, mitigation measures reduced NO_x emissions, but simultaneously increased primary emissions of f-NO_3^- (Feng et al., 2020; Palash et al., 2013; Tayyeb Javed et al., 2007; Yang et al., 2024; Zhao et al., 2020). As evidences presented in Sections 3.3, this phenomenon likely occurred across various Canadian urban atmospheres. In contrast, the second source in fresh cooling plumes is directly linked to NO_x emissions through the chemical conversion of NO_2 in cooling plume droplets, although it is highly sensitive to the lifetime of these droplets (Shen et al., 2022; Wang et al., 2016; Wang et al., 2020). In addition, primary nitrate aerosols from traffic emissions were reportedly unimportant in urban atmospheres across Canada and U.S. (Jeong et al., 2020; Chalbot et al., 2013), leaving only one possibility that primary nitrate aerosols were mainly derived from stationary combustion sources.

Although secondary f-NO_3^- formation should always occur to some extent in ambient air, the relative contribution from this process to the total f-NO_3^- is very small during the periods with high f-NO_3^- concentrations. As shown in Text S4 of SI, the modeled maximum potential contribution from secondary formation can only account for a small

fraction of the observed f-NO_3^- (<15% in the baseline runs, and <45% even in the empirical-estimate runs known to have overpredictions in general). These results support the hypothesis presented above that primary f-NO_3^- was the dominant contributor to the high f-NO_3^- concentration in winter. Moreover, higher f-NO_3^- concentrations were generally observed under low wind speeds (WS <1-2 m s^{-1}). Given that the sampling site is about 17 km from the farthest urban edge, the transport time for both primary and secondary f-NO_3^- to reach the site was therefore estimated to be approximately 2–4 h. This timescale is far too short for substantial secondary formation of f-NO_3^- in such cold ambient air (T < −10 °C), unless in-source processes dominated (Shen et al., 2022; USEPA, 2017; Zhang et al., 2023). Within this 2–4 h transport window, the amount of HNO_{3gas}* dry deposition should also be minimum, especially under low-temperature conditions.

3.6 Uncertainties affecting f-NO_3^- trends in Edmonton

Three categories of uncertainties that may affect the observed trends of f-NO_3^- in Edmonton were analyzed: (i) differences in observational results between the speciation sampler and the Dichotomous sampler, (ii) spatial inhomogeneity due to highly localized factors, and (iii) artifacts introduced by the sampling frequency (e.g., every third or sixth day), which may influence the calculation of annual averages. For category (i) uncertainty, $PM_{2.5}$ mass concentrations measured by the two different instruments at site S-90132 in 2010 showed strong agreement for most samples, with occasional discrepancies at lower concentration levels (Figure S6). Specifically, when the regression intercept was forced to zero, the resulting equation was $y = 1.02*x$ (R^2 = 0.94), and the difference in annual average concentrations was less than 10% (10.3 µg m^{-3} from the Dichotomous sampler vs. 11.1 µg m^{-3} from the speciation sampler).

For category (ii) uncertainty, Figure S7 compares real-time $PM_{2.5}$ mass concentrations measured simultaneously at two sites 7 km apart (S-90132 and S-90130) from 2011 to 2014. Other years were excluded due to significant data loss at one or both sites.

Regression slopes between the two sites (with intercepts forced to zero) are 0.86, 0.82, 0.58, and 0.67, with corresponding differences in annual average concentrations of 21%, 15%, 40%, and 39% in 2011, 2012, 2013, and 2014, respectively. The significant year-to-year differences between the two sites are unlikely caused by mitigation policies, climate variability, or changes in the atmospheric formation pathways of $PM_{2.5}$, but rather by spatial inhomogeneity driven by highly localized factors that varied from year to year (Yeganeh et al., 2025). The influence of such localized effects appears to be substantial and may represent an important, yet often overlooked, contributor to the disproportionately large decreases in the annual average f-NO_3^- relative to reductions in provincial total NO_x emissions over decadal timescales. More broadly, pronounced intra-urban spatial heterogeneity has been documented for many ionic aerosol components (with sulfate generally exhibiting a more regional character), underscoring the importance of high-resolution urban monitoring for interpreting long-term trends. At the same time, compared with routine PM mass measurements, sustained long-term, high-resolution chemical speciation monitoring requires substantially greater investment in instrumentation, maintenance, and operational resources, making such measurements more challenging to maintain over multi-year periods. This practical limitation highlights the need to carefully consider site representativeness and spatial heterogeneity when interpreting long-term nitrate trends derived from fixed-site observations.

It is noted that while the annual average $PM_{2.5}$ mass concentrations were significantly higher at S-90130 than S-90132 ($P < 0.01$) during 2010-2014, the opposite trend was observed for the annual average f-NO_3^-, e.g., higher at S-90132 during 2007–2019 compared to those at S-90130 during 1990–2005. The highest annual average f-NO_3^- concentration at S-90130 appeared in 2000 and that at S-90132 appeared in 2010 (Figure 1a). The mass fractions of f-NO_3^- in $PM_{2.5}$ were 0.050 ± 0.065 in 2000 and 0.13 ± 0.13 in 2010 (Figure S4), indicating that $PM_{2.5}$ at S-90132 contained more f-NO_3^- aerosols during 2007-2019 than at S-90130 during 1990-2005, strongly supporting the hypothesis that mitigation measures reduced NO_x emissions in Edmonton, while

simultaneously increased primary f-NO_3^- emissions from the first source (see Section 3.3) after 2005.

Concerning category (iii) uncertainty, no continuous measurements of f-NO_3^- were available to assess its magnitude. We thus used continuous measurements of $PM_{2.5}$ data at S-90130 as a proxy for this evaluation. Given that the annual average $PM_{2.5}$ mass concentration in 2010 was approximately 50% larger than in 2011, the analysis was conducted using data from 2011 to 2020 instead of 2010 to 2020. Daily average $PM_{2.5}$ mass concentrations were first calculated for every day of the year. Then for each year, annual average $PM_{2.5}$ mass concentrations were calculated from daily average concentrations using (i) full dataset, (ii) one in every three days data (three subsets), and (iii) one in every six days data (six subsets). Thus, a total of 10 sets of annual average $PM_{2.5}$ data series was created for the period of 2011-2020, which was then used for decadal trend analysis. The trend derived from the full dataset showed a decreasing trend with a Sen's Slope of 0.43 μg m^{-3} $year^{-1}$. Consistent decreasing trends were also obtained from using the one in every three days subset data series, with Sen's Slope values of 0.46, 0.46, and 0.42 μg m^{-3} $year^{-1}$, respectively, indicating an error of less than 8%. When using the one in every six days subset data series, five out of six data subsets also showed a decreasing trend, with Sen's Slope values of 0.47, 0.50, 0.45, 0.45, and 0.44 μg m^{-3} $year^{-1}$, respectively, indicating an error of less than 10% in most cases. However, one subset data series showed a probable decreasing trend, with a Sen's Slope of 0.38 μg m^{-3} $year^{-1}$.

Using the same approach described above, we also compared the decadal trends obtained from using one in every three days data, which are readily available, with those from using one in every six days data, which are arbitrarily split from the former data set into two subsets. One of the two subsets for f-NO_3^- showed a decreasing trend with a Sen's Slope of 0.055 μg m^{-3} $year^{-1}$, which is close to the original value of 0.063 μg m^{-3} $year^{-1}$; however, the other subset exhibited a stable trend. For f-SO_4^{2-}, both subsets showed decreasing trends, with Sen's Slope values of 0.033 and 0.018 μg m^{-3} $year^{-1}$,

755 respectively, although deviating to some extent from the original estimate of 0.022 μg
756 m^{-3} $year^{-1}$. For f-NH_4^+, both subsets showed stable trends, consistent with the results
757 derived from the original dataset. Overall, using one in every three or six days data can
758 generate decadal trends with reasonable accuracy, although the obtained trends need to
759 be interpreted carefully when the trends are not significant or the changing rates are
760 very small.
761
762 In the literature (Text S1 of SI), changes in atmospheric NH_3 and f-SO_4^{2-} have been
763 reported to influence long-term trends in f-NO_3 to some extent. However, evidence of
764 increasing atmospheric NH_3 in Canada, together with reduced NH_3 consumption for
765 neutralizing the two major inorganic acids, suggests that NH_3 is generally abundant and
766 unlikely to be the limiting factor for f-NO_3^- formation (Yao and Zhang, 2019).
767 Consistent with this interpretation, large f-NO_3^-/f-SO_4^{2-} mass ratios are frequently
768 observed in high-f-NO_3^- samples during the cold season across Canada. For example,
769 in Edmonton in 2010, samples with f-NO_3^- > 4 μg m^{-3} exhibited f-NO_3^-/f-SO_4^{2-} mass
770 ratios ranging from 1.5 to 12, with a median of 5.5. These results indicate that the
771 elevated f-NO_3^- concentrations overwhelmingly dominated its long-term trend. In such
772 cases, the slight decrease in f-SO_4^{2-} may exert only a minor influence on the trend in f-
773 NO_3^-. Nevertheless, these complex interactions warrant further investigation using
774 three-dimensional (3-D) air quality modelling; however, such efforts remain
775 challenging, as illustrated below.
776
777 Existing studies using 3-D chemical transport models (CTMs) simulating particulate
778 NO_3^- over North America are summarized in Text S5 of SI. Several key points can be
779 generated from these studies. (1) CTMs are widely applied and can often reproduce
780 broad spatial patterns and major controlling processes of particulate NO_3^- over the
781 United States and Canada; however, they frequently exhibit systematic biases in
782 magnitude, long-term trends, and sensitivities to emission controls, with a substantial
783 risk of error compensation (Pun et al., 2009; Smyth et al., 2009; Walker et al., 2012;
784 Kim et al., 2014, 2023; ECCC, 2016; Shah et al., 2018; Luo et al., 2019; Russell et al.,

2019; Pappin et al., 2024; Semeniuk et al., 2025). (2) The standard GEOS-Chem v12.0.0 simulation substantially overestimated surface $PM_{2.5}$ NO_3^- over the U.S. (1.89 μg m^{-3} vs. 0.70 μg m^{-3}), with pronounced spatial heterogeneity: outside California, the normalized mean bias reached +176%, whereas California exhibited an opposite bias of −62%, implying region-dependent dominant error sources (e.g., meteorology, emissions, and/or thermodynamics) (Walker et al., 2012; Luo et al., 2019). (3) simulated particulate NO_3^- often responds to NO_x controls in a strongly non-linear, and sometimes counterintuitive manner, posing a persistent "acidity–partitioning" challenge for trend attribution. For instance, in the northeastern United States, observations show that PM_{10} nitrate increased by 95% (urban) and 57% (rural) from 2005 to 2015 despite declining NO_x emissions, and this behavior was attributed to changes in aerosol acidity and gas–particle partitioning feedbacks that can offset the expected effect of precursor reductions (Kim et al., 2023). Finally, condensable particulate nitrate, as defined in US EPA Method 202 (US EPA, 2017), as well as its enhanced fraction under sub-freezing conditions, is generally not represented in current emission inventories. Given its potential importance, as suggested by our analysis presented above, incorporating temperature-dependent condensable nitrate into emission inventories is likely necessary to improve the representation and prediction of f-NO_3^- in 3-D air quality modelling.

4 Findings and implications

The in-depth analysis results presented in this study demonstrate that the dynamics of particulate nitrate in Canadian urban atmospheres are governed by complex interactions among emission reductions, primary sources, and cold-climate meteorology. Three key insights emerge:

(i) Non-linear responses of f-NO_3^- to NO_x emission reductions in all the cities: Early phase implementation of NO_x control measures paradoxically increased f-NO_3^- during

1998–2007, likely due to altered combustion plume chemistry favoring rapid f-NO_3^- formation in cold-climate conditions. Significant declines in f-NO_3^- (e.g., 60% in Edmonton) outpaced NO_x reductions in the most recent decade, driven by diminishing primary emissions, highly localized factors, and AO induced dispersion effects.

(ii) Decoupled c-NO_3^- and NO_x reductions in all the cities except Edmonton: c-NO_3^- remained stable or increased slightly while NO_x emissions were reduced. c-NO_3^- trends were likely controlled by the abundance of alkali aerosols, highlighting the limited efficacy of NO_x-focused policies for controlling c-NO_3^-.

(iii) Critical role of primary f-NO_3^- emissions in winter in all the cities: Over 80% of the annual f-NO_3^- burden was originated from cold-season primary emissions, with minimal contribution from secondary formation process, emphasizing the need for season-specific mitigation strategies. However, confirmation of this role requires three-dimensional air quality modeling with updated emission inventories that explicitly incorporate condensable particulate matter under subzero ambient temperatures.

Collectively, these findings call for a paradigm shift in air quality management. Effective mitigation strategies must explicitly address primary particulate nitrate sources, incorporate gas–particle partitioning dynamics under cold-climate conditions, and account for interactions with alkali-containing aerosols. Policy frameworks should further prioritize enhanced real-time measurements of $PM_{2.5}$ chemical composition to better resolve localized and seasonal variability, particularly in regions experiencing prolonged winter conditions. In parallel, coordinated unmanned aerial vehicle (UAV) and ground-based observations of CPM under contrasting temperature and atmospheric dispersion regimes are essential to provide direct observational evidence of its role and contributions.

Acknowledgement. QF and XY are supported by the Natural Science Foundation of China (grant no. 41776086). We greatly appreciate all the personnel of the NAPS Partners who operate the sites across Canada and collect the field samples, and the staff of the Analysis and Air Quality Section in Ottawa for the laboratory chemical analyses and QA/QC of the data used in the present study. NPRI/APEI groups are also acknowledged for their efforts in generating emissions data across Canada.

Data availability. The access of the data used in this study is described in Section 2 above.

Author Contributions. QF, XY and LZ designed the research, conducted the data analysis and wrote the manuscript.

Competing interests. One of the coauthors is a member of the editorial board of ACP.

References

Aas, W., Mortier, A., and Bowersox, V.et al.: Global and regional trends of atmospheric sulfur, Sci. Rep., 9, 953, 10.1038/s41598-018-37304-0, 2019.

Andersson, C., Langner, J., and Bergström, R.: Interannual variation and trends in air pollution over Europe due to climate variability during 1958–2001 simulated with a regional CTM coupled to the ERA40 reanalysis, Tellus Ser. B-Chem. Phys. Meteorol., 59, 77-98, 10.1111/j.1600-0889.2006.00196.x, 2007.

Balamurugan, V., Chen, J., and Qu, Z.et al.: Secondary $PM_{2.5}$ decreases significantly less than NO_2 emission reductions during COVID lockdown in Germany, Atmos. Chem. Phys., 22, 7105-7129, 10.5194/acp-22-7105-2022, 2022.

Bari, M. A., and Kindzierski, W. B.: Fine particulate matter ($PM_{2.5}$) in Edmonton, Canada: source apportionment and potential risk for human health, Environ. Pollut., 218, 219-229, 10.1016/j.envpol.2016.06.014, 2016a.

Bari, M. A., and Kindzierski, W. B.: Eight-year (2007–2014) trends in ambient fine particulate matter ($PM_{2.5}$) and its chemical components in the capital region of Alberta, Canada, Environ. Int., 91, 122-132, 10.1016/j.envint.2016.02.033, 2016b.

Bell, M. L., Dominici, F., and Ebisu, K.et al.: Spatial and temporal variation in $PM_{2.5}$ chemical composition in the United States for health effects studies, Environ. Health. Perspect., 115, 989-995, 10.1289/ehp.9621, 2007.

Bose, S., Rosa, M. J., and Mathilda Chiu, Y.et al.: Prenatal nitrate air pollution exposure and reduced child lung function: timing and fetal sex effects, Environ. Res., 167, 591-597, https://doi.org/10.1016/j.envres.2018.08.019, 2018.

Burakowski, E. A., Wake, C. P., Braswell, B., and Brown, D. P.: Trends in wintertime climate in the northeastern united states: 1965–2005, J. Geophys. Res. Atmos., 113, D20114,

10.1029/2008JD009870, 2008.

Canada Electricty Advisory Council: Powering Canada: A blueprint for success., 2024.

Chalbot, M. C., McElroy, B., and Kavouras, I. G.: Sources, trends and regional impacts of fine particulate matter in Southern Mississippi Valley: significance of emissions from sources in the Gulf of Mexico coast, Atmos. Chem. Phys., 13, 3721-3732, 10.5194/acp-13-3721-2013, 2013.

Chan, Y., Evans, M. J., and He, P.et al.: Heterogeneous nitrate production mechanisms in intense haze events in the North China Plain, J. Geophys. Res.-Atmos., 126, e2021JD034688, 10.1029/2021JD034688, 2021.

Chen, G., Fan, X., and Yu, S.et al.: HOCl formation driven by photochemical processes enhanced atmospheric oxidation capacity in a coastal atmosphere, Environ. Sci. Technol., 59, 5164-5171, 10.1021/acs.est.5c01363, 2025.

Cheng, B., Alapaty, K., and Arunachalam, S.: Spatiotemporal trends in $PM_{2.5}$ chemical composition in the conterminous U.S. During 2006–2020, Atmos. Environ., 316, 120188, 10.1016/j.atmosenv.2023.120188, 2024.

Cheng, I., and Zhang, L.: Long-term air concentrations, wet deposition, and scavenging ratios of inorganic ions, HNO_3, and so_2 and assessment of aerosol and precipitation acidity at Canadian rural locations, Atmos. Chem. Phys., 17, 4711-4730, 10.5194/acp-17-4711-2017, 2017.

Dabek-Zlotorzynska, E., Celo, V., and Ding, L.et al.: Characteristics and sources of $PM_{2.5}$ and reactive gases near roadways in two metropolitan areas in Canada, Atmos. Environ., 218, 116980, 10.1016/j.atmosenv.2019.116980, 2019.

Dabek-Zlotorzynska, E., Dann, T. F., and Kalyani Martinelango, P.et al.: Canadian national air pollution surveillance (NAPS) $PM_{2.5}$ speciation program: methodology and $PM_{2.5}$ chemical composition for the years 2003–2008, Atmos. Environ., 45, 673-686, 10.1016/j.atmosenv.2010.10.024, 2011.

Dang, R., Jacob, D. J., and Zhai, S.et al.: A satellite-based indicator for diagnosing particulate nitrate sensitivity to precursor emissions: application to East Asia, Europe, and North America, Environ. Sci. Technol., 58, 20101-20113, 10.1021/acs.est.4c08082, 2024.

Drugé, T., Nabat, P., Mallet, M., and Somot, S.: Model simulation of ammonium and nitrate aerosols distribution in the euro-mediterranean region and their radiative and climatic effects over 1979–2016, Atmos. Chem. Phys., 19, 3707-3731, 10.5194/acp-19-3707-2019, 2019.

Duce, R. A., LaRoche, J., and Altieri, K.et al.: Impacts of atmospheric anthropogenic nitrogen on the open ocean, Science, 320, 893-897, 10.1126/science.1150369, 2008.

ECCC: Canada – United States transboundary particulate matter science assessment 2013, 2016.

ECCC: Environment and climate change Canada: Canadian environmental sustainability indicators: air pollutant emissions, available at: https://www.canada.ca/en/environment-climate-change/services/environmental-indicators/air-pollutant-emissions.html, last access: 13 November 2021., in, edited,2021.

Edgerton, E. S., Hsu, Y., and White, E. M.et al.: Ambient concentrations and total deposition of inorganic sulfur, inorganic nitrogen and base cations in the Athabasca oil sands region, Sci. Total Environ., 706, 134864, 10.1016/j.scitotenv.2019.134864, 2020.

Fan, M., Zhang, Y., and Lin, Y.et al.: Changes of emission sources to nitrate aerosols in Beijing after the clean air actions: evidence from dual isotope compositions, J. Geophys. Res.-Atmos., 125, e2019JD031998, 10.1029/2019JD031998, 2020.

Feng, J., Chan, E., and Vet, R.: Air quality in the eastern united states and Eastern Canada for 1990–

2015: 25 years of change in response to emission reductions of SO2 and NOx in the region, Atmos. Chem. Phys., 20, 3107-3134, 10.5194/acp-20-3107-2020, 2020.

Font, A., de Brito, J. F., and Riffault, V.et al.: Long-term measurements of aerosol composition at rural background sites in France: sources, seasonality and mass closure of $PM_{2.5}$, Atmos. Environ., 334, 120724, 10.1016/j.atmosenv.2024.120724, 2024.

Gen, M., Liang, Z., and Zhang, R.et al.: Particulate nitrate photolysis in the atmosphere, Environmental Science: Atmospheres, 2, 111-127, 10.1039/d1ea00087j, 2022.

Guo, T., Li, K., and Zhu, Y.et al.: Concentration and size distribution of particulate oxalate in marine and coastal atmospheres – implication for the increased importance of oxalate in nanometer atmospheric particles, Atmos. Environ., 142, 19-31, 10.1016/j.atmosenv.2016.07.026, 2016.

Hand, J. L., Prenni, A. J., and Schichtel, B. A.: Trends in seasonal mean speciated aerosol composition in remote areas of the United States from 2000 through 2021, J. Geophys. Res.-Atmos., 129, e2023JD039902, 10.1029/2023JD039902, 2024.

Harrison, R. M., Beddows, D. C. S., Tong, C., and Damayanti, S.: Non-linearity of secondary pollutant formation estimated from emissions data and measured precursor-secondary pollutant relationships, npj Clim. Atmos. Sci., 5, 71, 10.1038/s41612-022-00297-9, 2022.

He, K., Yang, F., and Ma, Y.et al.: The characteristics of $PM_{2.5}$ in Beijing, China, Atmos. Environ., 35, 4959-4970, 10.1016/S1352-2310(01)00301-6, 2001.

Higgins, R. W., Leetmaa, A., and Kousky, V. E.: Relationships between climate variability and winter temperature extremes in the United States, J. Clim., 15, 1555-1572, 10.1175/1520-0442(2002)015<1555:RBCVAW>2.0.CO;2, 2002.

Höpfner, M., Ungermann, J., and Borrmann, S.et al.: Ammonium nitrate particles formed in upper troposphere from ground ammonia sources during Asian monsoons, Nat. Geosci., 12, 608-612, 10.1038/s41561-019-0385-8, 2019.

Huo, H., Gao, Y., and Sun, L.et al.: Investigating dual character of atmospheric ammonia on particulate NH_4NO_3: reducing evaporation versus promoting formation, Atmosphere, 16, 685, 10.3390/atmos16060685, 2025.

Iizuka, Y., Matsumoto, M., and Kawakami, K.et al.: Acidity-driven gas-particle partitioning of nitrate regulates its transport to arctic through the industrial era, Nat. Commun., 16, 4272, 10.1038/s41467-025-59208-0, 2025.

Jeong, C. H., McGuire, M. L., and Herod, D.et al.: Receptor model based identification of $PM_{2.5}$ sources in canadian cities, Atmos. Pollut. Res., 2, 158-171, 10.5094/APR.2011.021, 2011.

Jeong, C., Traub, A., and Huang, A.et al.: Long-term analysis of $PM_{2.5}$ from 2004 to 2017 in Toronto: composition, sources, and oxidative potential, Environ. Pollut., 263, 114652, 10.1016/j.envpol.2020.114652, 2020.

Jonson, J. E., Fagerli, H., Scheuschner, T., and Tsyro, S.: Modelling changes in secondary inorganic aerosol formation and nitrogen deposition in Europe from 2005 to 2030, Atmos. Chem. Phys., 22, 1311-1331, 10.5194/acp-22-1311-2022, 2022.

Kim, H., Walters, W. W., Kysela, L., and Hastings, M. G.: Long-term trends in inorganic aerosol chemical composition and chemistry at an urban and rural site in the Northeastern US, Sci. Total Environ., 904, 166848, 10.1016/j.scitotenv.2023.166848, 2023.

961 Kim, Y. J., Spak, S. N., and Carmichael, G. R.et al.: Modeled aerosol nitrate formation pathways during
962 wintertime in the Great Lakes region of North America, J. Geophys. Res.-Atmos., 119, 12, 412-420,
963 445, 10.1002/2014JD022320, 2014.
964 Li, Y., and Shiraiwa, M.: Timescales of secondary organic aerosols to reach equilibrium at various
965 temperatures and relative humidities, Atmos. Chem. Phys., 19, 5959-5971, 10.5194/acp-19-5959-
966 2019, 2019.
967 Lin, Y., Zhang, L., and Fan, Q.et al.: Decoupling impacts of weather conditions on interannual variations
968 in concentrations of criteria air pollutants in South China -- constraining analysis uncertainties by
969 using multiple analysis tools, Atmos. Chem. Phys., 22, 16073-16090, 10.5194/acp-22-16073-2022,
970 2022.
971 Luo, G., Yu, F., and Schwab, J.: Revised treatment of wet scavenging processes dramatically improves
972 GEOS-chem 12.0.0 simulations of surface nitric acid, nitrate, and ammonium over the United States,
973 Geosci. Model Dev., 12, 3439-3447, 10.5194/gmd-12-3439-2019, 2019.
974 Man, H., Zhu, Y., and Ji, F.et al.: Comparison of daytime and nighttime new particle growth at the
975 HKUST supersite in Hong Kong, Environ. Sci. Technol., 49, 7170-7178, 10.1021/acs.est.5b02143,
976 2015.
977 McDonald, B. C., de Gouw, J. A., and Gilman, J. B.et al.: Volatile chemical products emerging as largest
978 petrochemical source of urban organic emissions, Science, 359, 760-764, 10.1126/science.aaq0524,
979 2018.
980 Meng, Z., and Seinfeld, J. H.: Time scales to achieve atmospheric gas-aerosol equilibrium for volatile
981 species, Atmos. Environ., 30, 2889-2900, https://doi.org/10.1016/1352-2310(95)00493-9, 1996.
982 Palash, S. M., Masjuki, H. H., and Kalam, M. A.et al.: State of the art of NOx mitigation technologies
983 and their effect on the performance and emission characteristics of biodiesel-fueled compression
984 ignition engines, Energy Conv. Manag., 76, 400-420, 10.1016/j.enconman.2013.07.059, 2013.
985 Pappin, A. J., Charman, N., and Egyed, M.et al.: Attribution of fine particulate matter and ozone health
986 impacts in Canada to domestic and US emission sources, Sci. Total Environ., 909, 168529,
987 10.1016/j.scitotenv.2023.168529, 2024.
988 Park, R. J., Jacob, D. J., and Field, B. D.et al.: Natural and transboundary pollution influences on sulfate-
989 nitrate-ammonium aerosols in the United States: implications for policy, J. Geophys. Res. Atmos.,
990 109, 10.1029/2003JD004473, 2004.
991 Peng, W., Zhu, B., and Kang, H.et al.: Inconsistent 3-d structures and sources of sulfate ammonium and
992 nitrate ammonium aerosols during cold front episodes, J. Geophys. Res.-Atmos., 129,
993 e2023JD039958, 10.1029/2023JD039958, 2024.
994 Peng, X., Wang, T., and Wang, W.et al.: Photodissociation of particulate nitrate as a source of daytime
995 tropospheric cl2, Nat. Commun., 13, 939, 10.1038/s41467-022-28383-9, 2022.
996 Pullokaran, D., Bhardwaj, A., and Haswani, D.et al.: Spatio-temporal trends of the relationships between
997 surface $PM_{2.5}$ and its chemical constituents across three COALESCE network locations in India: a
998 mass closure investigation, J. Geophys. Res.-Atmos., 129, e2023JD039855, 10.1029/2023JD039855,
999 2024.

Pun, B. K., Balmori, R. T. F., and Seigneur, C.: Modeling wintertime particulate matter formation in central California, Atmos. Environ., 43, 402-409, 10.1016/j.atmosenv.2008.08.040, 2009.

Qi, J., Liu, X., and Yao, X.et al.: The concentration, source and deposition flux of ammonium and nitrate in atmospheric particles during dust events at a coastal site in Northern China, Atmos. Chem. Phys., 18, 571-586, 10.5194/acp-18-571-2018, 2018.

Russell, M., Hakami, A., and Makar, P. A.et al.: An evaluation of the efficacy of very high resolution air-quality modelling over the Athabasca oil sands region, Alberta, Canada, Atmos. Chem. Phys., 19, 4393-4417, 10.5194/acp-19-4393-2019, 2019.

Seinfeld, J. H., and Pandis, S. N.: Atmospheric chemistry and physics: from air pollution to climate change. Third edition. Hoboken, new jersey: John Wiley & Sons, inc., in, edited,2016.

Semeniuk, K., Dastoor, A., and Lupu, A.: Implementation of the MOSAIC aerosol module (v1.0) in the Canadian air quality model GEM-MACH (v3.1), Geosci. Model Dev., 18, 6479-6515, 10.5194/gmd-18-6479-2025, 2025.

Shah, V., Jaeglé, L., and Thornton, J. A.et al.: Chemical feedbacks weaken the wintertime response of particulate sulfate and nitrate to emissions reductions over the eastern united states, Proc. Natl. Acad. Sci., 115, 8110-8115, 10.1073/pnas.1803295115, 2018.

Shen, Y., Meng, H., and Yao, X.et al.: Does ambient secondary conversion or the prolonged fast conversion in combustion plumes cause severe $PM_{2.5}$ air pollution in China? Atmosphere, 13, 673, 10.3390/atmos13050673, 2022.

Sickles II, J. E., and Shadwick, D. S.: Air quality and atmospheric deposition in the eastern US: 20 years of change, Atmos. Chem. Phys., 15, 173-197, 10.5194/acp-15-173-2015, 2015.

Smyth, S. C., Jiang, W., and Roth, H.et al.: A comparative performance evaluation of the AURAMS and CMAQ air-quality modelling systems, Atmos. Environ., 43, 1059-1070, 10.1016/j.atmosenv.2008.11.027, 2009.

Squizzato, S., Masiol, M., Rich, D. Q., and Hopke, P. K.: $PM_{2.5}$ and gaseous pollutants in New York state during 2005–2016: spatial variability, temporal trends, and economic influences, Atmos. Environ., 183, 209-224, 10.1016/j.atmosenv.2018.03.045, 2018.

Statistics Canada: New motor vehicle registrations, fourth quarter 2023, The Daily, released 12 March 2024, available at: https://www150.statcan.gc.ca/n1/daily-quotidien/240312/dq240312c-eng.htm (last access: 24 February 2026), 2024.

Sun, P., Wang, J., and Liu, Y.et al.: Enhanced particulate nitrate formation in residual layer exacerbates near-surface pollution: insights from tethered airship and long-term ground measurements, J. Geophys. Res.-Atmos., 130, e2024JD042672, 10.1029/2024JD042672, 2025.

Sun, W., Shao, M., and Granier, C.et al.: Long-term trends of anthropogenic so, NO, CO, and NMVOCs emissions in China, Earth's Future, 6, 1112-1133, 10.1029/2018EF000822, 2018.

Tang, Y. S., Braban, C. F., and Dragosits, U.et al.: Acid gases and aerosol measurements in the UK (1999--2015): regional distributions and trends, Atmos. Chem. Phys., 18, 16293-16324, 10.5194/acp-18-16293-2018, 2018.

Tayyeb Javed, M., Irfan, N., and Gibbs, B. M.: Control of combustion-generated nitrogen oxides by

selective non-catalytic reduction, J. Environ. Manage., 83, 251-289, 10.1016/j.jenvman.2006.03.006, 2007.

Thunis, P., Clappier, A., and Beekmann, M.et al.: Non-linear response of $PM_{2.5}$ to changes in NOx and NH_3 emissions in the po basin (Italy): consequences for air quality plans, Atmos. Chem. Phys., 21, 9309-9327, 10.5194/acp-21-9309-2021, 2021.

USEPA: Method 202—dry impinger method for determining condensable particulate emissions from stationary sources, Emission Measurement Center, Research Triangle Park, NC, USA, 2017.

Velazquez-Garcia, A., Crumeyrolle, S., and de Brito, J. F.et al.: Deriving composition-dependent aerosol absorption, scattering and extinction mass efficiencies from multi-annual high time resolution observations in northern France, Atmos. Environ., 298, 119613, 10.1016/j.atmosenv.2023.119613, 2023.

Walker, J. M., Philip, S., Martin, R. V., and Seinfeld, J. H.: Simulation of nitrate, sulfate, and ammonium aerosols over the United States, Atmos. Chem. Phys., 12, 11213-11227, 10.5194/acp-12-11213-2012, 2012.

Wang, G., Zhang, R., and Gomez, M. E.et al.: Persistent sulfate formation from London fog to Chinese haze, Proc. Natl. Acad. Sci., 113, 13630-13635, 10.1073/pnas.1616540113, 2016.

Wang, H., Wang, H., and Lu, X.et al.: Increased night-time oxidation over China despite widespread decrease across the globe, Nat. Geosci., 16, 217-223, 10.1038/s41561-022-01122-x, 2023.

Wang, H., Zhang, L., and Cheng, I.et al.: Spatiotemporal trends of $PM_{2.5}$ and its major chemical components at urban sites in Canada, J. Environ. Sci., 103, 1-11, 10.1016/j.jes.2020.09.035, 2021.

Wang, M., Kong, W., and Marten, R.et al.: Rapid growth of new atmospheric particles by nitric acid and ammonia condensation, Nature, 581, 184-189, 10.1038/s41586-020-2270-4, 2020.

Wang, M., Xiao, M., and Bertozzi, B.et al.: Synergistic HNO_3–h_2so_4–NH_3 upper tropospheric particle formation, Nature, 605, 483-489, 10.1038/s41586-022-04605-4, 2022.

Ward, R. X., Baliaka, H. D., and Schulze, B. C.et al.: Poorly quantified trends in ammonium nitrate remain critical to understand future urban aerosol control strategies, Sci. Adv., 11, eadt8957, 10.1126/sciadv.adt8957, 2025.

Wernis, R. A., Kreisberg, N. M., and Weber, R. J.et al.: Source apportionment of VOCs, IVOCs and SVOCs by positive matrix factorization in suburban Livermore, California, Atmos. Chem. Phys., 22, 14987-15019, 10.5194/acp-22-14987-2022, 2022.

Wetherbee, G. A., and Mast, M. A.: Annual variations in wet-deposition chemistry related to changes in climate, Clim. Dyn., 47, 3141-3155, 10.1007/s00382-016-3017-7, 2016.

Wexler, A. S., and Seinfeld, J. H.: The distribution of ammonium salts among a size and composition dispersed aerosol, Atmospheric Environment. Part A. General Topics, 24, 1231-1246, https://doi.org/10.1016/0960-1686(90)90088-5, 1990.

Wexler, A. S., and Seinfeld, J. H.: Analysis of aerosol ammonium nitrate: departures from equilibrium during SCAQS, Atmospheric Environment. Part A. General Topics, 26, 579-591, https://doi.org/10.1016/0960-1686(92)90171-G, 1992.

Xiao, H., Chen, T., and Zhang, Q.et al.: Changes in the dominant contributions of nitrate formation and sources during haze episodes: insights from dual isotopic evidence, J. Geophys. Res.-Atmos., 130, e2024JD042175, 10.1029/2024JD042175, 2025.

Yan, C., Tham, Y. J., and Nie, W.et al.: Increasing contribution of nighttime nitrogen chemistry to wintertime haze formation in Beijing observed during COVID-19 lockdowns, Nat. Geosci., 16, 975-

981, 10.1038/s41561-023-01285-1, 2023.
Yang, L., Shi, Y., and Luo, L.: Review of emission characteristics of fine particles during coal-fred SCR DeNOx process, Proc. Chin. Soc. Electr. Eng., 36, 4342-4348, 10.7666/d.Y2782597, 2016.
Yang, T., Li, H., and Xu, W.et al.: Strong impacts of regional atmospheric transport on the vertical distribution of aerosol ammonium over Beijing, Environ. Sci. Technol. Lett., 11, 29-34, 10.1021/acs.estlett.3c00791, 2024.
Yao, X., Lau, A. P. S., and Fang, M.et al.: Size distributions and formation of ionic species in atmospheric particulate pollutants in Beijing, China: 1—inorganic ions, Atmos. Environ., 37, 2991-3000, 10.1016/S1352-2310(03)00255-3, 2003.
Yao, X., Lee, C. J., and Evans, G. J.et al.: Evaluation of ambient so_2 measurement methods at roadside sites, Atmos. Environ., 45, 2781-2788, 10.1016/j.atmosenv.2011.01.070, 2011.
Yao, X., and Zhang, L.: Chemical processes in sea-salt chloride depletion observed at a canadian rural coastal site, Atmos. Environ., 46, 189-194, 10.1016/j.atmosenv.2011.09.081, 2012a.
Yao, X., and Zhang, L.: Supermicron modes of ammonium ions related to fog in rural atmosphere, Atmos. Chem. Phys., 12, 11165-11178, 10.5194/acp-12-11165-2012, 2012b.
Yao, X., and Zhang, L.: Causes of large increases in atmospheric ammonia in the last decade across North America, ACS Omega, 4, 22133-22142, 10.1021/acsomega.9b03284, 2019.
Yao, X., and Zhang, L.: Decoding long-term trends in the wet deposition of sulfate, nitrate, and ammonium after reducing the perturbation from climate anomalies, Atmos. Chem. Phys., 20, 721-733, 10.5194/acp-20-721-2020, 2020.
Yao, X., and Zhang, L.: Identifying decadal trends in deweathered concentrations of criteria air pollutants in Canadian urban atmospheres with machine learning approaches, Atmos. Chem. Phys., 24, 7773-7791, 10.5194/acp-24-7773-2024, 2024.
Yeganeh, B., Shakerdonyavi, A., Zafarmomen, N., and Taheri, A.: Comprehensive spatiotemporal analysis of long-term mobile monitoring for traffic-related particles in a complex urban environment, Atmos. Pollut. Res., 102870, 10.1016/j.apr.2025.102870, 2025.
Zaveri, R. A., Easter, R. C., and Singh, B.et al.: Development and evaluation of chemistry-aerosol-climate model CAM5-chem-MAM7-MOSAIC: global atmospheric distribution and radiative effects of nitrate aerosol, J. Adv. Model. Earth Syst., 13, e2020MS002346, 10.1029/2020MS002346, 2021.
Zhai, S., Jacob, D. J., and Wang, X.et al.: Control of particulate nitrate air pollution in China, Nat. Geosci., 14, 389-395, 10.1038/s41561-021-00726-z, 2021.
Zhang, L., Vet, R., and Wiebe, A.et al.: Characterization of the size-segregated water-soluble inorganic ions at eight Canadian rural sites, Atmos. Chem. Phys., 8, 7133-7151, 10.5194/acp-8-7133-2008, 2008.
Zhang, Q., Wang, Y., and Liu, M.et al.: Wintertime formation of large sulfate particles in China and implications for human health, Environ. Sci. Technol., 57, 20010-20023, 10.1021/acs.est.3c05645, 2023.
Zhang, Z., Li, Y., and Zhang, X.et al.: Review of hazardous materials in condensable particulate matter, Fuel Process. Technol., 220, 106892, 10.1016/j.fuproc.2021.106892, 2021.
Zhao, S., Hu, B., and Gao, W.et al.: Effect of the “coal to gas” project on atmospheric NO_X during the heating period at a suburban site between Beijing and Tianjin, Atmos. Res., 241, 104977, 10.1016/j.atmosres.2020.104977, 2020.
Zhou, M., Nie, W., and Qiao, L.et al.: Elevated formation of particulate nitrate from n_2o_5 hydrolysis in the Yangtze River Delta region from 2011 to 2019, Geophys. Res. Lett., 49, e2021GL097393, 10.1029/2021GL097393, 2022.

Zhu, Y., Sabaliauskas, K., and Liu, X.et al.: Comparative analysis of new particle formation events in less and severely polluted urban atmosphere, Atmos. Environ., 98, 655-664, 10.1016/j.atmosenv.2014.09.043, 2014.

List of Figures

Figure 1. (a) Annual variations of mass concentrations of f-NO_3^- and c-NO_3^- in Edmonton, (b) annual variations of mixing ratio of NO_2 in Edmonton and provincial total NO_x emissions, (c) f-NO_3^- and c-NO_3^- at S-90130 vs. NO_x emissions, (d) f-NO_3^- and c-NO_3^- in Winnipeg, (e) NO_2 mixing ratio in Winnipeg and provincial total NO_x emissions, and time series of 24-h integrated f-NO_3^- and c-NO_3^- in 1996 (f) and 2007 (g) at a time resolution of one sample in every three days. Blue and black markers in (a) represent data obtained at S-90130 and S-90132 in Edmonton, respectively. Blue and black markers in (d) represent data points in Winnipeg before and after 2003, respectively. Dashed lines in (c) denote least-squares regression fits for f-NO_3^- and c-NO_3^-.

Figure 2. (a) Annual variations of mass concentrations of f-NO_3^- and c-NO_3^- in Quebec City, (b) annual variations of mixing ratio of NO_2 in Quebec City and provincial total NO_x emissions, (c) f-NO_3^- and c-NO_3^- in Montreal, (d) NO_2 mixing ratio in Montreal, (e) f-NO_3^- and c-NO_3^- in Victoria, (f) NO_2 mixing ratio in Victoria, (g) f-NO_3^- and c-NO_3^- in Vancouver, and (h) NO_2 mixing ratio in Vancouver. Blue and black markers in (a) represent data points before and after 2003, respectively. Blue and black markers in (c), (e), and (g) represent data points before and after 2002, respectively.

Figure 3. Single-factor (T, WS, RH, and HNO_{3gas}^*) effects on daily f-NO_3^- (and HNO_3^* in the case of T factor) in 2010 and 2015.

Figure 4. Time series of 24-h integrated f-NO_3^- in 2010 (a) and 2015 (b) in Edmonton at a time resolution of one sample in every three days, and correlations in the re-constructed f-NO_3^- between 2015 and 2010 using data points with values of full range (0^{th}-100^{th} percentiles) (c), central 50% (25^{th}-75^{th} percentile) (d), and lower 50% (0^{th}-50^{th} percentile) (e).

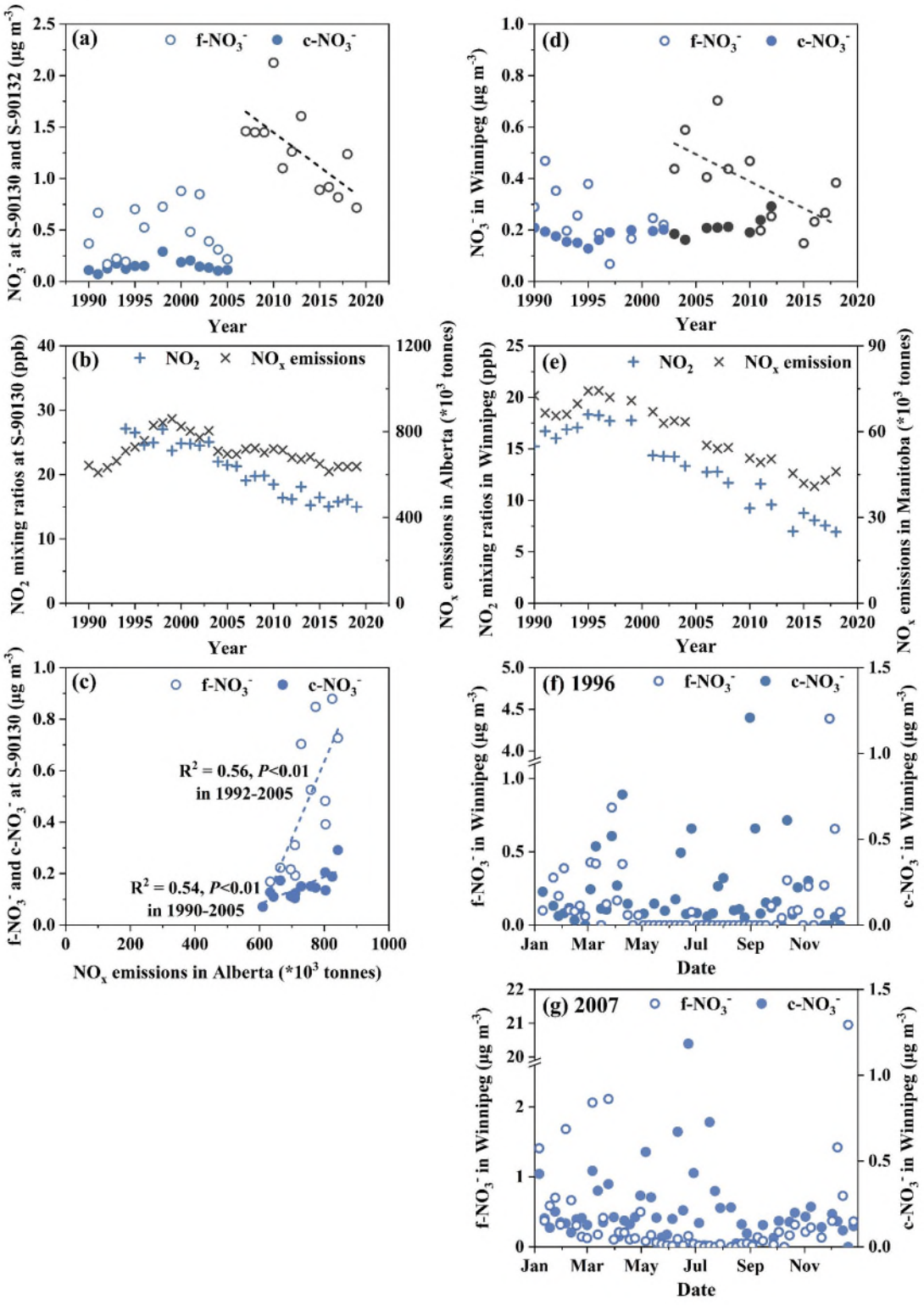

Figure 1. (a) Annual variations of mass concentrations of f-NO_3^- and c-NO_3^- in Edmonton, (b) annual variations of mixing ratio of NO_2 in Edmonton and provincial total NO_x emissions, (c) f-NO_3^- and c-NO_3^- at S-90130 vs. NO_x emissions, (d) f-NO_3^-

and c-NO_3^- in Winnipeg, (e) NO_2 mixing ratio in Winnipeg and provincial total NO_x emissions, and time series of 24-h integrated f-NO_3^- and c-NO_3^- in 1996 (f) and 2007 (f) at a time resolution of one sample in every three days. Blue and black markers in (a) represent data obtained at S-90130 and S-90132 in Edmonton, respectively. Blue and black markers in (d) represent data points in Winnipeg before and after 2003, respectively. Dashed lines in (c) denote least-squares regression fits for f-NO_3^- and c-NO_3^-.

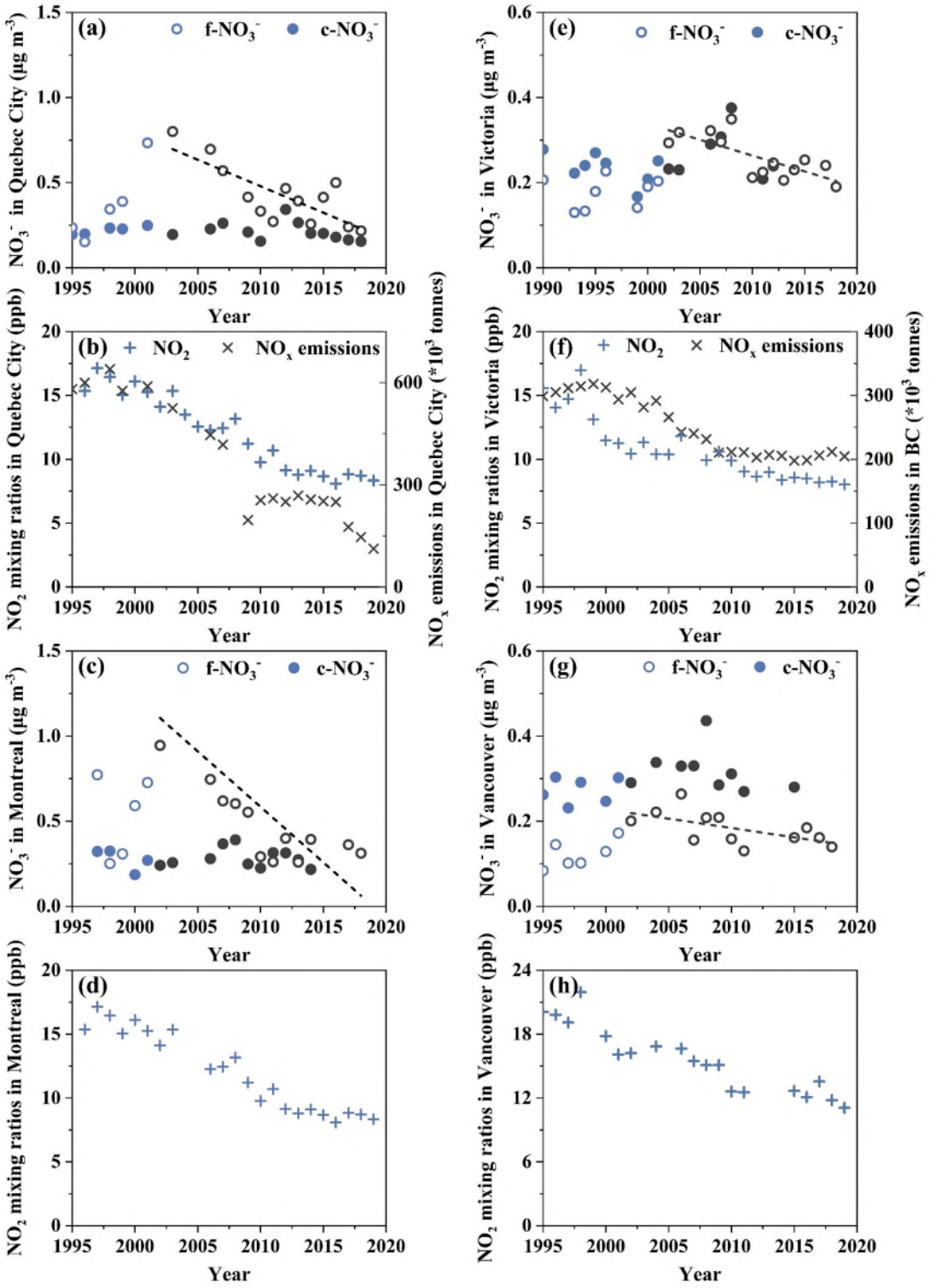

Figure 2. (a) Annual variations of mass concentrations of f-NO_3^- and c-NO_3^- in Quebec City, (b) annual variations of mixing ratio of NO_2 in Quebec City and provincial total NO_x emissions, (c) f-NO_3^- and c-NO_3^- in Montreal, (d) NO_2 mixing ratio in Montreal, (e) f-NO_3^- and c-NO_3^- in Victoria, (f) NO_2 mixing ratio in Victoria, (g) f-NO_3^- and c-

NO_3^- in Vancouver, and (h) NO_2 mixing ratio in Vancouver. Blue and black markers in (a) represent data points before and after 2003, respectively. Blue and black markers in (c), (e), and (g) represent data points before and after 2002, respectively.

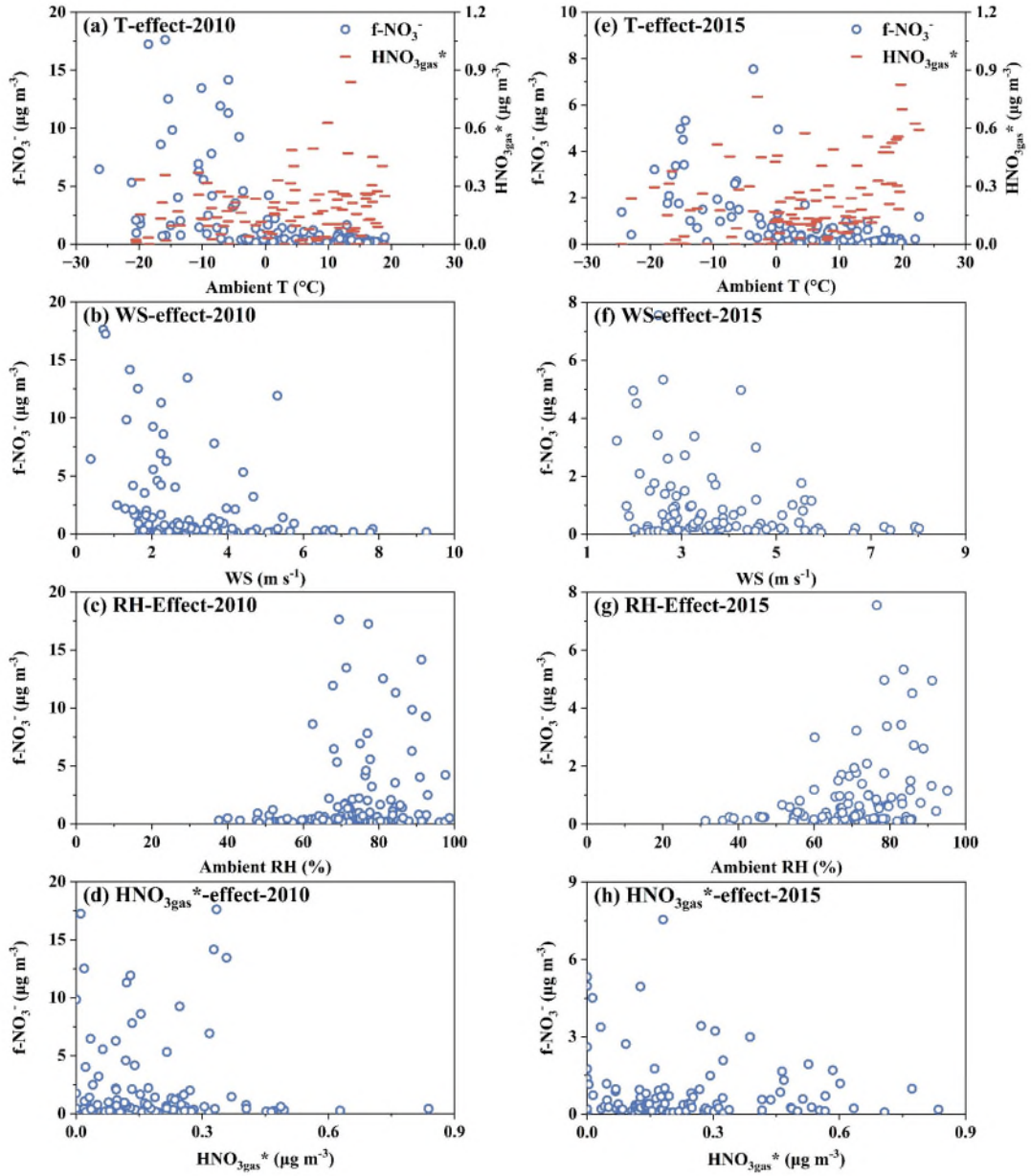

Figure 3. Single-factor (T, WS, RH, and HNO_{3gas}^*) effects on daily f-NO_3^- (and HNO_3^* in the case of T factor) in 2010 and 2015.

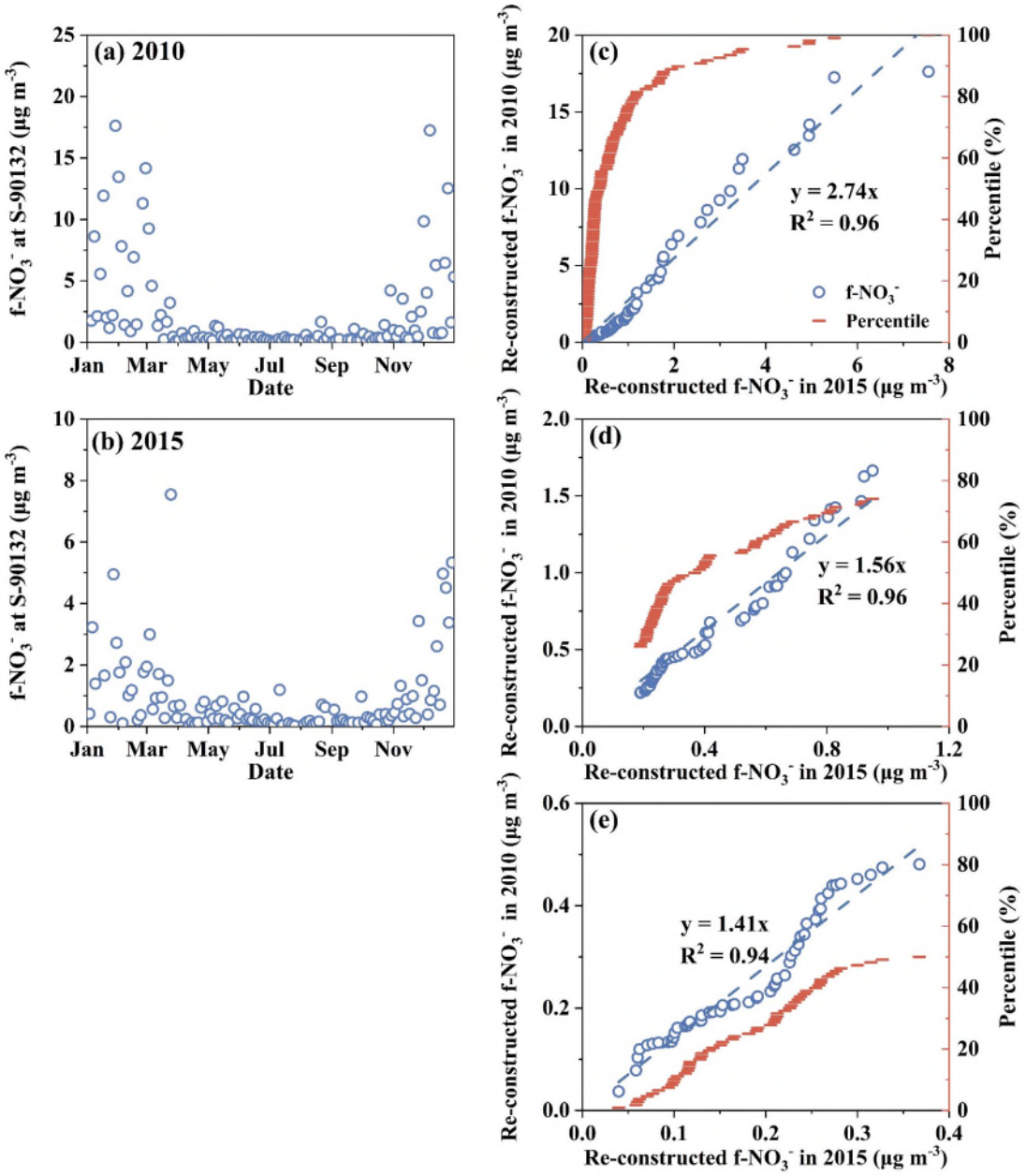

Figure 4. Time series of 24-h integrated f-NO_3^- in 2010 (a) and 2015 (b) in Edmonton at a time resolution of one sample in every three days, and correlations in the re-constructed f-NO_3^- between 2015 and 2010 using data points with values of full range (0^{th}-100^{th} percentiles) (c), central 50% (25^{th}-75^{th} percentile) (d), and lower 50% (0^{th}-50^{th} percentile) (e).

Supplement Information

Novel insights on causes of disproportionate trends between particulate NO_3^- and NO_x emissions in Canadian urban atmospheres

Qinchu Fan et al.

Correspondence to: Xiaohong Yao (xhyao@ouc.edu.cn), Leiming Zhang (leiming.zhang@ec.gc.ca)

This file contains six Text sections, two Tables, and eight Figures.

The copyright of individual parts of the supplement might differ from the article licence.

Text S1. A brief review of literature-reported long-term trends in particulate nitrate in response to NO_x emission reductions in Canada, the United States, Europe, and China

Within Canada, long-term observations indicate that trends in inorganic aerosols are neither spatially uniform nor monotonic. For example, in Toronto, both nitrate (NO_3^-) and sulfate (SO_4^{2-}) in $PM_{2.5}$ (particles < 2.5 μm) declined rapidly during 2004–2017 (-6.9% yr^{-1} and -8.1% yr^{-1}, respectively), accompanied by decreases in ammonium (NH_4^+) (Jeong et al., 2020). In contrast, in Edmonton (2007–2014), neither $PM_{2.5}$ nor the major inorganic ions (NO_3^-, SO_4^{2-}, NH_4^+) exhibited statistically significant trends (Bari and Kindzierski, 2016).

At a broader rural and non-urban scale, data collected through the Canadian Air and Precipitation Monitoring network (CAPMoN) (1988–2007) revealed distinct non-monotonic annual variations in particulate NO_3^- in total suspended particle (TSP): approximately stable during 1988–1993, increasing during 1993–2002, and declining during 2002–2007. Site-to-site differences suggest strong modulation by meteorology, long-range transport, and aerosol thermodynamics in addition to precursor emissions (Zbieranowski and Aherne, 2012).

This asymmetry between particulate SO_4^{2-} and NO_3^- responses becomes clearer at the eastern North American scale. During 1990–2015, SO_2 emissions fell sharply (−84% in the eastern U.S.; −66% in eastern Canada), while NO_x reductions were more modest (−54% and −22%, respectively). Corresponding, SO_4^{2-} and NH_4^+ in TSP decreased substantially (−73.3% and −67.4%), whereas NO_3^- decreased by only −29.1% (largely after 2000), indicating that NO_3^- responds more weakly and more conditionally to emission controls than SO_4^{2-} and NH_4^+.

Winter-focused analyses further illustrate why NO_{3-} can resist or even offset expected declines. Shah et al. (2018) compared winter conditions in 2007 and 2015 and found that, despite substantial reductions in winter SO_2 (-58%) and NO_x (−35%) emissions, winter $PM_{2.5}$ NO_3^- showed little change. Similarly, a detailed analysis at paired urban and rural sites in Rhode Island (northeastern U.S.) reported pronounced increases in NO_3^- in PM_{10} (particle < 10 μm) during 2005–2015 (+95% urban; +57%

rural) despite substantial SO_2 and NO_x emission reductions, consistent with acidity- and partitioning-driven feedbacks that can partially counteract NO_x controls (Kim et al., 2023).

In line with the findings described above, early NO_x-control phases were sometimes accompanied by rising particulate NO_3^- across the eastern U.S. For example, NO_3^- in TSP increased by 11% from 1990–1994 to 2000–2004 (winter: 31%) even as NO_x emissions declined by 22% (Sickles II and Shadwick, 2015). Similarly, at several CAPMoN sites (ALG, LON, EGB, and KEJ) in Canada, NO_3^- in TSP increased significantly during 1993-2002 followed by declines during 2002-2007 (Zbieranowski and Aherne, 2011). These findings underscore the nonlinear and phase-dependent response of nitrate to precursor controls.

Comparable non-linearities have also been documented in other fast-changing regions. In Europe, EMEP assessments report >80% reductions in SO_x and ~50% reductions in NO_x, but only ~12% reductions in NH_3 during 2000–2019. Correspondingly, particulate SO_4^{2-} in TSP declined at ~3–4% yr^{-1}, whereas total nitrate (HNO_{3gas} + particulate NO_3^-) decreased more slowly at ~1.5–2% yr^{-1} (Aas et al., 2024). Observations in the United Kingdom further illustrate phase-dependent decoupling: at two London sites, NO_3^- in PM_{10} changed only slightly during 2012–2018 and became largely stagnant after 2014, despite continued significant declines in ambient NO_x and NO_2; meanwhile, rural AGANET measurements (2000-2020) show that NO_3^- in TSP decreased at 2.12% yr^{-1}, significantly slower than the decline in NO_x emissions (2.84% yr^{-1}) and rural NO_x concentrations (3.48% yr^{-1}), implying an increasing nitrate-to-precursor ratio over time and highlighting the roles of NH_3 availability, thermodynamic partitioning, and regional transport (Harrison et al., 2022).

In contrast, under aggressive SO_2 controls in North China (2008–2016), SO_2, NO_x and NH_3 emissions decreased by −60%, −16% and −7%, respectively (Liu et al., 2018). Nevertheless, $PM_{2.5}$ NO_3^- increased by ~28%, accompanied by a ~30% rise in gas-phase NH_3, underscoring how shifts in aerosol acidity and NH_3 availability can redirect inorganic aerosol composition and even promote nitrate under certain control

phases (Liu et al., 2018).

The cross-regional comparisons presented in this section underscore the inherently nonlinear behavior of particulate nitrate trends. This complexity calls for a regionally focused Canadian synthesis that explicitly accounts for the coupled evolution of SO_2, NO_x, and NH_3 emissions, thermodynamic partitioning processes, and meteorological variability when interpreting long-term f-NO_3^- trends.

Text S2. Analysis of the relative importance of 15 major variables on f-NO_3^- formation using a Random Forest model

The Random Forest (RF) model embedded in the *"ranger"* R package was used here to simulate the nonlinear relationship between daily f-NO_3^- and a suite of 15 predictor variables (Wright and Ziegler, 2017; Schmid et al., 2016). These predictors include NO_2 and $PM_{2.5}$ concentrations; near-surface meteorological variables including wind speed and direction (WS, WD), relative humidity (RH), temperature (T), dew point, visibility, and surface pressure; boundary-layer height (BLH); surface shortwave radiation (SSR); total cloud cover (TCC); total precipitation (TP); and two seasonal timing variables. The two seasonal timing variables was encoded with two Fourier terms—sin and cos of day-of-year (DOY)—to capture the annual cycle without year-end discontinuity.

Hourly WS, WD, RH, T, surface pressure, dew point, and visibility were obtained from the Edmonton International Airport station via *"worldMet"* R package and aggregated to daily means. Daily BLH, SSR, TCC, and TP were sourced from ERA5 (Copernicus Climate Data Store) and harmonized to time zone-specific daily values. The model was trained using a randomly selected 70% subset of data from 2010–2019, with the remaining 30% data reserved for model performance evaluation (Fig. S8a). Sensitivity tests indicated that selecting 1,000 trees with a minimum node size of 6 provided stable performance.

For the 30% test data set, the ordinary-least-squares slope of predicted versus observed values was 0.54, with MSE = 1.2 μg m^{-3}, MAE = 0.42 μg m^{-3}, and R^2 = 0.68. Permutation-based variable importance (Fig. S8b) ranked predictors in

ascending order of importance from top to bottom. Temperature emerged as the most influential variable (Importance ≈ 0.114), followed by $PM_{2.5}$ (0.064), NO_2 (0.061), and BLH (0.052). Moisture metrics (dew point 0.037; RH 0.013) and SSR (0.021) were moderately informative. Transport- and optics-related variables also contribute to some extent (WD, 0.013; WS, 0.007; visibility, 0.011), though less strongly than the leading predictors mentioned above. In contrast, cloud, precipitation, and pressure played minimum role on the daily scale (TCC, 0.003; TP, 0.002; pressure, 0.002).

Partial dependence plots (PDPs) for the top three predictors identified by permutation importance (T, $PM_{2.5}$, and NO_2) (Fig. S8c–e) show a strong non-linear relationship between predicted f-NO_3^- and temperature, characterized by a sharp decline around 0°C. In contrast, $PM_{2.5}$ and NO_2 display threshold-like increases followed by saturation, suggesting that cold conditions strongly favor particulate nitrate persistence, whereas the impacts of pollution intensity and NO_x-related indicators are modulated and ultimately constrained by other limiting factors.

Text S3. Simulation of secondary f-NO_3^- formation using the Flexible 0-D Atmospheric Model (F0AM)

The Flexible 0-D Atmospheric Model (F0AM) with the CB6r2 chemical mechanism was used to simulate f-NO_3^- formation on ten days with f-NO_3^- concentration higher than 9 μg m^{-3} in 2010 (00:00–23:00 local time), results from which can quantify the maximum retainable secondary f-NO_3^- (Luecken et al., 2019; Wolfe et al., 2016). Simulations were run in MATLAB with a 1-h external step (adaptive internal sub-stepping) and full time-series output. The box model was constrained by the observed NO_2, O_3, and CO; all other species evolved freely. To avoid numerical instability, initial conditions were set to NO = 10^{-4} ppb and HNO_3 = 10^{-3} ppb. Meteorological inputs including surface pressure (P), temperature (T), relative humidity (RH), and solar zenith angle (SZA) were computed from site latitude/longitude and local time. Surface albedo was fixed at 0.1. Photolysis frequencies followed F0AM's SZA-driven parameterization using a TOMS-like total O_3 column from OMI/Aura Level-3 (OMTO3d, 1°×1°) retrieved via NASA GES DISC Giovanni and interpolated to the

model time resolution. The dilution constant k_{dil} was inferred from CO as a quasi-conservative tracer. HNO_3 dry deposition was represented as $k_{dep}=(v_d/100)/H$, where v_d is the dry-deposition velocity (cm s^{-1}) and H is the boundary-layer height (m).

From model reaction rates we diagnosed total gas-phase HNO_3 production P_{gas} and the $OH + NO_2 \rightarrow HNO_3$ channel P_{OH}. Nighttime heterogeneous N_2O_5 hydrolysis was included as a diagnostic upper bound and applied only when SZA > 90°:

$$P_{N_2O_5}^{het} = Yk_{het}[N_2O_5] \quad (1)$$

$$k_{het} = \frac{\gamma \bar{c} S_A}{4} \quad (2)$$

where Y is the stoichiometric HNO_3 yield per N_2O_5 uptake, γ is the uptake coefficient of N_2O_5 (removal probability of N_2O_5 per collision with the wet aerosol surface), $\bar{c}$ is the mean molecular speed of N_2O_5, and S_A is the aerosol surface area concentration.

Over each 24-h window we integrated total chemical production and diagnostic losses:

$$P_{chem} = \int (P_{gas} + P_{N_2O_5}^{het})dt \quad (3)$$

$$P_{loss} = \int (k_{dil}[HNO_3]^+ + k_{dep}[HNO_3])dt \quad (4)$$

where P_{gas} is the total gas-phase HNO_3 production rate (ppb s^{-1}), and $[HNO_3]^+$ = max ($[HNO_3] - [HNO_3]_{bkg}$, 0) with $[HNO_3]_{bkg}$ = 0 to provide a local-increment upper bound. The retainable upper bound of secondary particulate nitrate was then calculated as:

$$NO_{3\,sec,max}^- = \alpha \max(P_{chem} - P_{loss}, 0) \quad (5)$$

where α converts ppb to μg m^{-3} for nitrate using the daily mean T and P. To avoid double counting, $P_{N_2O_5}^{het}$ (Eq. 1) was added only if the gas-phase mechanism lacked an explicit $N_2O_5 \rightarrow HNO_3$ pathway.

In a baseline configuration designed to represent a typical mid-latitude winter urban setting (γ = 0.01, S_A=200 , Y=1.5; Mielke et al., 2016; Zang et al., 2022), the retainable secondary particulate nitrate was 2.5 μg m^{-3} on January 19, 2010 (the highest observed f-NO_3^- in 2010) and 0.3 μg m^{-3} on December 7, 2010 (the second highest observed f-NO_3^- in 2010) , corresponding to 14% and 1.4% of observed f-

NO_3^-, respectively (Table S2a). Using empirical estimates of aerosol surface area derived from $PM_{2.5}$ with RH growth and T (S_A=583 and 554 for 2010-01-29 and 2010-12-07; γ held at 0.01), the retainable secondary burden increased to 4.4 and 6.7 μg m^{-3}, i.e., 25% and 39%, respectively, of the observed values (Table S2b). The latter parameters, however, resulted in the predicted f-NO_3^- to as high as 86 μg m^{-3} on February 28, 2010, which were six times of the observed value and is practically impossible in Canada. Thus, all predicted values larger than the observations were excluded for further analysis.

When examining the well-behaved simulation cases in Table S2ab, all predicated values were substantially smaller than the observations, except for 1 December 2010 (S_A=338 and γ at 0.015). Even in the empirical-estimate cases, where predictions are generally larger, the contribution of retainable secondary particulate nitrate never exceeds 45% of the observed f-NO_3^-. Overall, the test results suggested that the primary f-NO_3^- dominantly contributed to the higher values of f-NO_3^- in winter.

Text S4. Description of the hypothesis: Was the observed f-NO_3^- entirely derived from the condensation of HNO_{3gas}* in Canadian urban atmospheres during the cold season?

To test the hypothesis if the observed f-NO_3^- was entirely derived from the condensation of HNO_{3gas}* (≈HNO_{3gas} + N_2O_{5gas}) in Canadian urban atmospheres during the cold season, we first analyzed the 20 daily samples in 2010 with f-NO_3^- concentration of > 4 μg m^{-3} (out of 116 total samples that year). For these 20 samples, the mass ratios of f-NO_3^- to HNO_{3gas} varied from 21 to >100, with a median value of 63.

Assuming that the observed f-NO_3^- was entirely derived from the condensation of HNO_{3gas}* (≈HNO_{3gas} + N_2O_{5gas}), mass conservation requires that the net production of f-NO_3^- equal the net loss of HNO_{3gas}^*. Because the observed concentrations of f-NO_3^- were one to two orders of magnitude higher than those of HNO_{3gas}^*, this hypothesis implicitly requires a quasi-static condition for HNO_{3gas}^* (i.e., $d[HNO_{3gas}^*]/dt \approx 0$). Such a condition would imply that the rapid formation of HNO_{3gas}^* is balanced by its

removal through conversion into f-NO_3^-. Similar quasi-static approximations are commonly applied in the literature to infer concentrations of highly reactive species (e.g., OH radicals).

However, the daily time resolution of our dataset does not permit direct estimation of f-NO_3^- formation rates. Therefore, we evaluated the hypothesis indirectly. If the condition $d[HNO_{3gas}^*]/dt \approx 0$ accompanied with the balanced rapid formation and removal of HNO_{3gas}^* does not hold for the 20 samples, the above hypothesis fails. If the removal rate of HNO_{3gas}^* approaches zero while its formation remains rapid, the concentration of HNO_{3gas}^* would be expected to increase substantially. Under such circumstances, low concentrations of f-NO_3^- should be associated with a low removal rate of HNO_{3gas}^* in the process of f-NO_3^- formation. Thus, the examination of $d[HNO_{3gas}^*]/dt \approx 0$ accompanied with the balanced rapid formation and removal of HNO_{3gas}^* is further reframed into testing a weaker hypothesis: whether HNO_{3gas}^* concentrations significantly increased under conditions with low f-NO_3^- concentrations, compared to cases with high f-NO_3^- concentrations. Such an increase would be necessary, but not sufficient to accept the quasi-static approximation. Conversely, if no such increase was observed, the hypothesis must be rejected, i.e., the observed low concentrations of HNO_{3gas}^* could not have given rise to high f-NO_3^- concentrations prior to their detection at the sampling site, based on the principle of mass conservation.

Text S5. A brief review of the overall performance of particulate nitrate modeling in Canada and the United States.

S5.1. Overall model performance and the "error compensation" challenge in simulating particulate nitrate

Chemical transport models (CTMs; e.g., AURAMS, CMAQ, GEOS-Chem, and GEM-MACH) have been widely used to simulate particulate nitrate (NO_3^-) and generally reproduce the broad spatial patterns and key controlling processes across Canada and the U.S. However, they frequently exhibit systematic biases in concentration magnitude, long-term trends, and sensitivities to emission controls,

along with a substantial risk of "error compensation" (Pun et al., 2009; Smyth et al., 2009; Walker et al., 2012; Kim et al., 2014, 2023; ECCC, 2016; Shah et al., 2018; Luo et al., 2019; Russell et al., 2019; Pappin et al., 2024; Semeniuk et al., 2025).

Multi-model evaluations highlight pronounced regional heterogeneity in model errors and the potential of an "illusion of good agreement" in total PM mass. For example, the standard GEOS-Chem v12.0.0 simulation substantially overestimated surface $PM_{2.5}$ NO_3^- over the U.S. (1.89 μg m^{-3} vs. 0.70 μg m^{-3}), with strong spatial heterogeneity: outside California the normalized mean bias (NMB) reached +176%, whereas California showed an opposite bias (−62%), implying region-dependent dominant error sources (meteorology, emissions, or thermodynamics) (Walker et al., 2012; Luo et al., 2019). Even in high-resolution simulations for California's San Joaquin Valley (CMAQ-MADRID), $PM_{2.5}$ NO_3^- was overestimated by 35%, indicating that uncertainties in emissions and gas–particle partitioning can be amplified under local conditions (Pun et al., 2009).

Cross-model comparisons further demonstrate that "getting PM mass right" does not guarantee correct composition: although both AURAMS and CMAQ v4.6 underestimated total $PM_{2.5}$ in July 2002, CMAQ performed better for the nitrate component than AURAMS, suggesting that different models may achieve similar total mass through compensating errors among individual components (Smyth et al., 2009).

Importantly, condensable particulate NO_3^-, as defined by the U.S. EPA (2016), as well as its enhanced fraction under freezing ambient conditions, remains absent from current emission inventories. Incorporating this component could be critical for improving the performance of particulate NO_3^- simulations, particularly during cold winter seasons across Canada and the northern United States.

S5.2. Imbalance in regional research depth: intensive mechanism-based studies in the U.S. versus limited Canada-focused assessments

A notable gap lies in the uneven depth of regional investigation. In the U.S., numerous studies have conducted systematic, quantitative evaluations and mechanistic

decomposition of particulate NO_3^-. In some of these studies, CTM simulations relevant to Canada treat the country within a broader North American or primarily as part of transboundary analyses. In contrast, relatively few stand-alone, Canada-focused assessments provide detailed quantitative attribution and process-level evaluation (Pappin et al., 2024; ECCC, 2016).

Existing modeling efforts over the Canadian domain generally fall into three categories, each reflecting the broader CTM challenges noted above:

(1) Operational model development: Advancements in Canada's operational CTM (GEM-MACH), including updates such as incorporation of the MOSAIC aerosol module, demonstrate that particulate NO_3^- is highly sensitive to dry deposition parameterizations. Earlier model configurations also lacked key processes (e.g., heterogeneous hydrolysis of N_2O_5), limiting performance in simulating wintertime particulate NO_3^- (Semeniuk et al., 2025).

(2) High-resolution simulations over major source regions: Nested, high-resolution simulations targeting industrial hotspots (e.g., oil sands regions) indicate that finer spatial resolution improves representation of plume peaks. However, conventional site-based evaluation metrics may be "masked" by small wind-direction biases and uncertainties in emission spatial allocation, complicating interpretation of localized chemical processes (Russell et al., 2019).

(3) Uncertainty in transboundary attribution: Studies quantifying the contribution of U.S. emissions to Canada's $PM_{2.5}$-related health burden emphasize that chemical nonlinearity, particularly for NO_3^-, can substantially amplify uncertainties in scenario-based approaches (e.g., zero-out methods) (Pappin et al., 2024).

S5.3. Key mechanism constraints: removal processes, heterogeneous chemistry, and thermodynamics

Across both Canada and the U.S., accurately representing physical removal and chemical formation pathways is essential for simulating particulate NO_3^-. On the physical side, improved wet-scavenging parameterizations, such as incorporating time-varying in-cloud condensate and scavenging rates, can substantially enhance

model performance. In GEOS-Chem, for example, such updates reduced the annual mean simulated particulate NO_3^- in the U.S. from 1.89 to 0.88 μg m^{-3}, underscoring that wet removal can constrain fine NH_4NO_3 as strongly as chemical production does (Luo et al., 2019).

Mechanistically, wintertime $PM_{2.5}$ NO_3^- is highly sensitive to nocturnal heterogeneous chemistry. Process-level diagnostics indicate that winter production of $PM_{2.5}$ NO_3^- in the U.S. Midwest is dominated by heterogeneous N_2O_5 conversion (~57%), followed by OH + NO_2 reactions (~28%) (Kim et al., 2014). In rural California, approximately two-thirds of $PM_{2.5}$ NO_3^- formation is likewise attributed to heterogeneous pathways (Pun et al., 2009).

Importantly, particulate NO_3^- responds to NO_x controls in a strongly nonlinear manner and may even exhibit counterintuitive trends, posing a persistent "acidity–partitioning" challenge for long-term simulations. Between 2005 and 2015 in the northeastern U.S., PM_{10} NO_3^- increased by 95% in urban areas and 57% in rural areas despite declining NO_x emissions; modeling attributed this pattern to shifts in aerosol acidity and gas–particle partitioning that offset the expected benefits of precursor reductions (Kim et al., 2023). Analyses using GEOS-Chem further suggest that substantial SO_2 reductions from 2007 to 2015 decreased aerosol acidity (i.e., increased pH), thereby favoring partitioning of HNO_3 into the particle phase and diminishing the marginal effectiveness of NO_x controls for reducing particulate NO_3^- (Shah et al., 2018).

This thermodynamic feedback also helps explain why chemical transport models may underestimate observed nitrate declines. For example, CMAQ simulated much weaker decreases (−0.4% to −0.5% yr^{-1}) than those observed (−2.1% to −2.5% yr^{-1}) and failed to capture interannual variability (Xing et al., 2015). Over a 25-year period, total inorganic nitrate (TNO_3) declined by 52.6%, whereas particulate $PM_{2.5}$ NO_3^- decreased by only 29.1%, further demonstrating a delayed and conditional response governed by evolving neutralization efficiency and partitioning dynamics (Feng et al., 2020).

S5.4. Summary and implications

Overall, uncertainties in model simulated particulate NO_3^- are governed by three primary factors: (1) emission inventories**,** particularly biases in NH_3 and NO_x that propagate through both chemical production and deposition pathways; (2) **k**ey chemical and thermodynamic parameters, including $\gamma(N_2O_5)$ and aerosol pH sensitivity; and (3) physical processes and model resolution, such as simplified wet-removal schemes and biases in nighttime boundary-layer height.

Future research should move beyond simply "matching $PM_{2.5}$ mass" and instead adopt a multi-constraint framework that jointly evaluates particle size distributions, acidity–partitioning diagnostics (e.g., pH and TNO_3), heterogeneous chemistry (e.g., N_2O_5 uptake), and seasonal NH_3 variability. In particular, sensitivity analyses should explicitly identify the conditions under which NO_x controls become less effective due to acidity-driven partitioning shifts. Doing so would elevate nitrate trend attribution and health-benefit assessments from empirical model fitting to mechanistically testable science.

Notably, condensable particulate NO_3^-, as defined by the U.S. EPA (2017), and its enhanced fraction under freezing ambient conditions are not currently included in emission inventories. Given their demonstrated importance in this study, these components should be urgently incorporated into inventories to improve the accuracy of f-NO_3^- predictions in 3-D air quality models.

References

Aas, W.; Fagerli, H.; Alastuey, A.; Cavalli, F.; Degorska, A.; Feigenspan, S.; Brenna, H.; Gliß, J.; Heinesen, D.; Hueglin, C.; Holubová, A.; Jaffrezo, J.; Mortier, A.; Murovec, M.; Putaud, J.; Rüdiger, J.; Simpson, D.; Solberg, S.; Tsyro, S.; Tørseth, K.; Yttri, K.E. Trends in air pollution in Europe, 2000–2019. *Aerosol Air Qual. Res.* **2024**, *24*, 230237.

Bari, M.A.; Kindzierski, W.B. Eight-year (2007–2014) trends in ambient fine particulate matter ($PM_{2.5}$) and its chemical components in the capital region of Alberta, Canada. *Environ. Int.* **2016**, *91*, 122-132.

ECCC, Canada – United States Transboundary Particulate Matter Science Assessment 2013. 2016.

Feng, J.; Chan, E.; Vet, R. Air quality in the eastern united states and Eastern Canada for 1990–2015: 25 years of change in response to emission reductions of SO_2 and NO_x in the region. *Atmos. Chem. Phys.* **2020**, *20*, 3107-3134.

Harrison, R.M.; Beddows, D.C.S.; Tong, C.; Damayanti, S. Non-linearity of secondary pollutant formation estimated from emissions data and measured precursor-secondary pollutant relationships. *Npj Clim. Atmos. Sci.* **2022**, *5*, 71.

Jeong, C.; Traub, A.; Huang, A.; Hilker, N.; Wang, J.M.; Herod, D.; Dabek-Zlotorzynska, E.; Celo, V.; Evans, G.J. Long-term analysis of $PM_{2.5}$ from 2004 to 2017 in Toronto: composition, sources, and oxidative potential. *Environ. Pollut.* **2020**, *263*, 114652.

Kim, H.; Walters, W.W.; Kysela, L.; Hastings, M.G. Long-term trends in inorganic aerosol chemical composition and chemistry at an urban and rural site in the northeastern US. *Sci. Total Environ.* **2023**, *904*, 166848.

Kim, Y.J.; Spak, S.N.; Carmichael, G.R.; Riemer, N.; Stanier, C.O. Modeled aerosol nitrate formation pathways during wintertime in the great lakes region of North America. *J. Geophys. Res.-Atmos.* **2014**, *119*, 12, 412-420, 445.

Liu, M.; Huang, X.; Song, Y.; Xu, T.; Wang, S.; Wu, Z.; Hu, M.; Zhang, L.; Zhang, Q.; Pan, Y.; Liu, X.; Zhu, T. Rapid so_2 emission reductions significantly increase tropospheric ammonia concentrations over the North China Plain. *Atmos. Chem. Phys.* **2018**, *18*, 17933-17943.

Luecken, D.J.; Yarwood, G.; Hutzell, W.T. Multipollutant modeling of ozone, reactive nitrogen and HAPs across the continental US with CMAQ-CB6. *Atmos. Environ.* **2019**, *201*, 62-72.

Luo, G.; Yu, F.; Schwab, J. Revised treatment of wet scavenging processes dramatically improves GEOS-chem 12.0.0 simulations of surface nitric acid, nitrate, and ammonium over the United States. *Geosci. Model Dev.* **2019**, *12*, 3439-3447.

Mielke, L.H.; Furgeson, A.; Odame-Ankrah, C.A.; Osthoff, H.D. Ubiquity of ClNO2 in the urban boundary layer of Calgary, Alberta, Canada. *Can. J. Chem.* **2016**, *94*, 414-423.

Pappin, A.J.; Charman, N.; Egyed, M.; Blagden, P.; Duhamel, A.; Miville, J.; Popadic, I.; Manseau, P.M.; Marcotte, G.; Mashayekhi, R.; Racine, J.; Rittmaster, R.; Edwards, B.; Kipusi, W.; Smith-Doiron, M. Attribution of fine particulate matter and ozone health impacts in Canada to domestic and US emission sources. *Sci. Total Environ.* **2024**, *909*, 168529.

Pun, B.K.; Balmori, R.T.F.; Seigneur, C. Modeling wintertime particulate matter formation in central California. *Atmos. Environ.* **2009**, *43*, 402-409.

Russell, M.; Hakami, A.; Makar, P.A.; Akingunola, A.; Zhang, J.; Moran, M.D.; Zheng, Q. An evaluation of the efficacy of very high resolution air-quality modelling over the Athabasca oil sands region, Alberta, Canada. *Atmos. Chem. Phys.* **2019**, *19*, 4393-4417.

Schmid, M.; Wright, M.N.; Ziegler, A. On the use of Harrell's c for clinical risk prediction via random survival forests. *Expert Syst. Appl.* **2016**, *63*, 450-459.

Semeniuk, K.; Dastoor, A.; Lupu, A. Implementation of the MOSAIC aerosol module (v1.0) in the Canadian air quality model GEM-MACH (v3.1). *Geosci. Model Dev.* **2025**, *18*, 6479-6515.

Shah, V.; Jaeglé, L.; Thornton, J.A.; Lopez-Hilfiker, F.D.; Lee, B.H.; Schroder, J.C.; Campuzano-Jost, P.; Jimenez, J.L.; Guo, H.; Sullivan, A.P.; Weber, R.J.; Green, J.R.; Fiddler, M.N.; Bililign, S.; Campos, T.L.; Stell, M.; Weinheimer, A.J.; Montzka, D.D.; Brown, S.S. Chemical feedbacks weaken the wintertime response of particulate sulfate and nitrate to emissions reductions over the eastern united states. *Proc. Natl. Acad. Sci.* **2018**, *115*, 8110-8115.

Sickles II, J.E.; Shadwick, D.S. Air quality and atmospheric deposition in the eastern US: 20 years of change. *Atmos. Chem. Phys.* **2015**, *15*, 173-197.

Smyth, S.C.; Jiang, W.; Roth, H.; Moran, M.D.; Makar, P.A.; Yang, F.; Bouchet, V.S.; Landry, H. A comparative performance evaluation of the AURAMS and CMAQ air-quality modelling systems. *Atmos. Environ.* **2009**, *43*, 1059-1070.

US EPA, Method 202—Dry Impinger Method for Determining Condensable Particulate Emissions from Stationary Sources. 2017.

Walker, J.M.; Philip, S.; Martin, R.V.; Seinfeld, J.H. Simulation of nitrate, sulfate, and ammonium aerosols over the United States. *Atmos. Chem. Phys.* **2012**, *12*, 11213-11227.

Wolfe, G.M.; Marvin, M.R.; Roberts, S.J.; Travis, K.R.; Liao, J. The framework for 0-d atmospheric modeling (F0AM) v3.1. *Geosci. Model Dev.* **2016**, *9*(9), 3309-3319.

Wright, M.N.; Ziegler, A. Ranger: a fast implementation of random forests for high dimensional data in C++ and r. *J. Stat. Softw.* **2017**, *77*(1), 1-17.

Xing, J.; Mathur, R.; Pleim, J.; Hogrefe, C.; Gan, C.M.; Wong, D.C.; Wei, C.; Gilliam, R.; Pouliot, G. Observations and modeling of air quality trends over 1990–2010 across the northern hemisphere: China, the United States and Europe. *Atmos. Chem. Phys.* **2015**, *15*(5), 2723-2747.

Zang, H.; Zhao, Y.; Huo, J.; Zhao, Q.; Fu, Q.; Duan, Y.; Shao, J.; Huang, C.; An, J.; Xue, L.; Li, Z.; Li, C.; Xiao, H. High atmospheric oxidation capacity drives wintertime nitrate pollution in the Eastern Yangtze River Delta of China. *Atmos. Chem. Phys.* **2022**, *22*(7), 4355-4374.

Zbieranowski, A.L.; Aherne, J. Long-term trends in atmospheric reactive nitrogen across Canada: 1988–2007. *Atmos. Environ.* **2011**, *45*(32), 5853-5862.

Zbieranowski, A.L.; Aherne, J. Spatial and temporal concentration of ambient atmospheric ammonia in Southern Ontario, Canada. *Atmos. Environ.* **2012**, *62*, 441-450.

Table S1. Information on pollutant concentrations, meteorological variables, and emissions datasets for each Canadian site.

City (Site)	Variable	Time span (Time resolution)
Edmonton (S-90132)	f-NO_3^- (μg m^{-3})	2007-2019 (with 2014 missing, 3-day)
	f-SO_4^{2-} (μg m^{-3})	2007-2019 (with 2014 missing, 3-day)
	f-NH_4^+ (μg m^{-3})	2007-2019 (with 2014 missing, 3-day)
	$PM_{2.5}$ (μg m^{-3})	2010-2014 (1-hr)
Edmonton (S-90130)	f-NO_3^- (μg m^{-3})	1990-2005 (with 1997 and 1999 missing, 6-day)
	c-NO_3^- (μg m^{-3})	1990-2005 (with 1997 and 1999 missing, 6-day)
	f-SO_4^{2-} (μg m^{-3})	1990-2005 (with 1997 and 1999 missing, 6-day)
	f-NH_4^+ (μg m^{-3})	1992-2005 (with 1997 and 1999 missing, 6-day)
	NO_2 mixing ratio (ppb)	1994-2019 (1-hr)
	$PM_{2.5}$ concentration (μg m^{-3})	2011-2014 (1-hr)
	HNO_{3gas} (μg m^{-3})	2010, 2015 (1-day)
	NO_x emissions (*10^3 tones)	1990-2019 (1-yr)
	SO_2 emissions (*10^3 tones)	1990-2019 (1-yr)
	NH_3 emissions (*10^3 tones)	1990-2019 (1-yr)
	T (℃)	2010, 2015 (1-day)
	WS (m s^{-1})	2010, 2015 (1-day)
	RH (%)	2010, 2015 (1-day)
Winnipeg	f-NO_3^- (μg m^{-3})	1990-2018 (with 1998, 2000, 2005, 2009, 2013, 2014 missing, 6-day)
	c-NO_3^- (μg m^{-3})	1990-2012 (with 1998, 2000, 2005, 2009 missing,6-day)
	NO_2 mixing ratio (ppb)	1990-2019 (1-hr)
	NO_x emissions (*10^3 tones)	1990-2018 (1-yr)
Quebec City	f-NO_3^- (μg m^{-3})	1995-2018 (with 1997, 2000, 2002, 2004, 2005, 2008 missing, 6-day)
	c-NO_3^- (μg m^{-3})	1995-2018 (with 1997, 2000, 2002, 2004, 2005, 2008 missing, 6-day)
	NO_2 mixing ratio (ppb)	1996-2019 (1-hr)
	NO_x emissions (*10^3 tones)	1995-2019 (1-yr)
Montreal	f-NO_3^- (μg m^{-3})	1997-2018 (with 2004, 2005, 2015, and 2016 missing, 6-day)
	c-NO_3^- (μg m^{-3})	1997-2014 (with 2004 and 2005 missing, 6-day)
	NO_2 mixing ratio (ppb)	1996-2019 (1-hr)
Hamilton	f-NO_3^- (μg m^{-3})	1995-2019 (with 2003, 2004, and 2011 missing, 3-day)
	c-NO_3^- (μg m^{-3})	1998-2012 (with 2003, 2004, and 2011 missing, 3-day)
	NO_2 mixing ratio (ppb)	1996-2019 (1-hr)
	NO_x emissions (*10^3 tones)	1995-2019 (1-yr)
Victoria	f-NO_3^- (μg m^{-3})	1990-2018 (with 1991, 1992, 1997, 1998, 2004, 2005, 2009, and 2016 missing, 6-day)
	c-NO_3^- (μg m^{-3})	1990-2012 (with 1991, 1992, 1997, 1998, 2004, 2005, 2009, and 2010 missing, 6-day)
	NO_2 mixing ratio (ppb)	1993-2019 (1-hr)
	NO_x emissions (*10^3 tones)	1990-2019 (1-yr)
Vancouver	f-NO_3^- (μg m^{-3})	1990-2018 (with 1992, 1994, 1999, 2003, 2005, and 2012-2014 missing, 6-day)
	c-NO_3^- (μg m^{-3})	1990-2012 (with 1992, 1994, 1999, 2003, 2005, and 2012-2014 missing, 6-day)
	NO_2 mixing ratio (ppb)	1990-2019 (1-hr)

Table S2. Sensitivity of the retainable upper bound secondary f-NO_3^- (f-$NO_{3\ sec,\ max}^-$) to the uptake coefficient of N_2O_5 (γ) and aerosol surface area concentration (S_A) on ten days in 2010 with f-NO_3^- concentration > 9 μg m^{-3}, evaluated with the F0AM box model.

Date	f-$NO_{3\ obs}^-$ (μg m^{-3})	γ	S_A (μm^2 cm^{-3})	P_{chem} (ppb)	P_{OH} (ppb)	$P_{N_2O_5}$ (ppb)	P_{loss} (ppb)	f-$NO_{3\ sec,\ max}^-$ (μg m^{-3})
2010/01/29	18	0.010	200	2	0.3	2	1	2
2010/12/07	17	0.010	200	1	0.2	0.8	1	0.3
2010/12/25	13	0.010	200	3	0.3	2	2	2
2010/02/25	11	0.010	200	3	1	2	8	0
2010/03/03	9	0.010	200	13	2	11	14	0
2010/01/08	9	0.010	200	1	0.2	0.9	1	0
2010/02/28	14	0.010	200	33	2	30	18	43
2010/02/01	13	0.010	200	13	0.6	13	8	14
2010/01/17	12	0.010	200	27	0.7	25	4	64
2010/12/01	10	0.010	200	7	0.3	7.0	2	15
2010/01/29	18	0.01	583	3	0.3	2	1	4
2010/12/07	17	0.01	554	3	0.2	3	1	7
2010/12/25	13	0.015	478	4	0.3	4	2	5
2010/01/17	12	0.01	95	6	0.7	4	4	5
2010/12/01	10	0.015	338	5	0.3	5	2	8
2010/01/08	9	0.01	182	1	0.2	0.8	1	0
2010/02/28	14	0.015	558	48	2	46	18	86
2010/02/01	13	0.01	360	16	0.6	15	8	22
2010/02/25	11	0.015	513	16	1	14	8	23
2010/03/03	9	0.015	513	13	2	11	10	10

- f-$NO_{3\ obs}^-$, the observed f- NO_3^- concentration; P_{chem}, total chemical production of f-NO_3^-; P_{OH}, production of f-NO_3^- via $OH+NO_2 \rightarrow HNO_3$; $P_{N_2O_5}$, production of f-NO_3^- by nighttime heterogeneous N_2O_5 hydrolysis; P_{loss}, losses of f-NO_3^- via dilution and dry deposition.
- The top block reports day-specific γ and S_A estimates and the bottom block shows a baseline representative of a mid-latitude winter urban setting (γ = 0.01, S_A=200).

Cells highlighted in orange indicate cases where f-$NO_{3\ sec,\ max}^-$ exceeds f-$NO_{3\ obs}^-$.

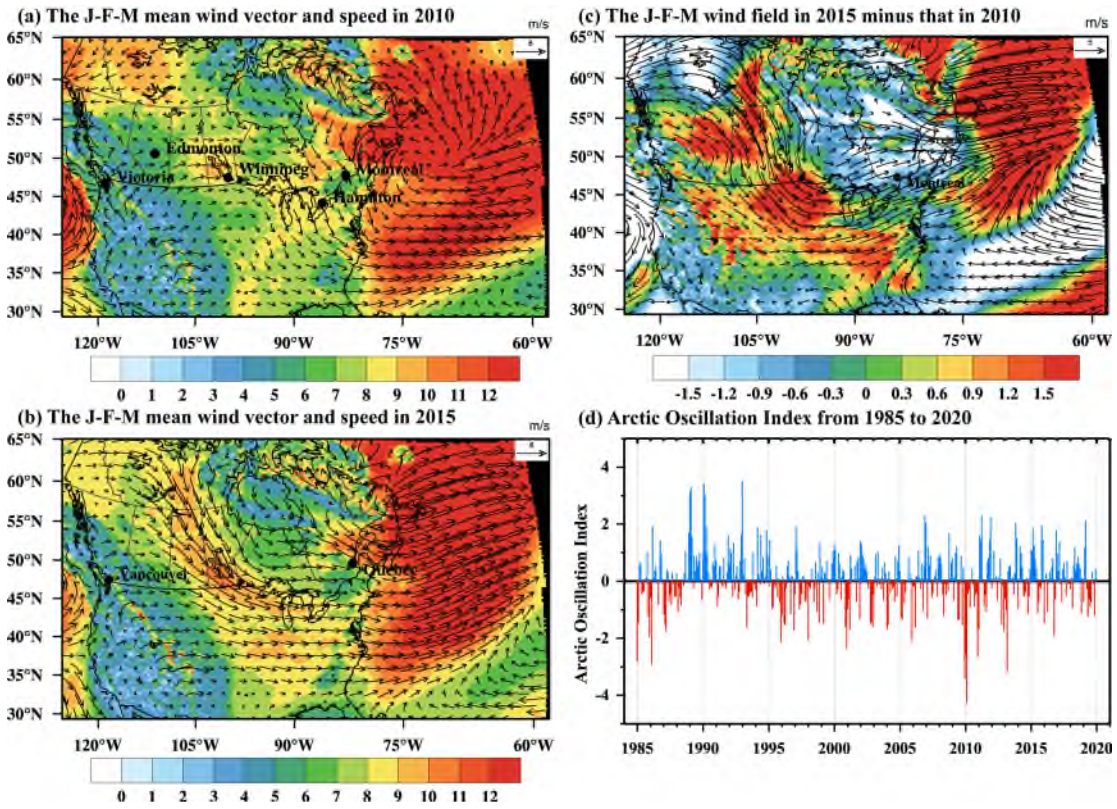

Figure S1. Mean wind vector in January-February-March (JFM) in 2010 (a) and 2015 (b), the difference in the JFM mean wind vector between 2010 and 2015 (2015 minus 2010) (c), and Arctic Oscillation Index from 1990 to 2020 (d)

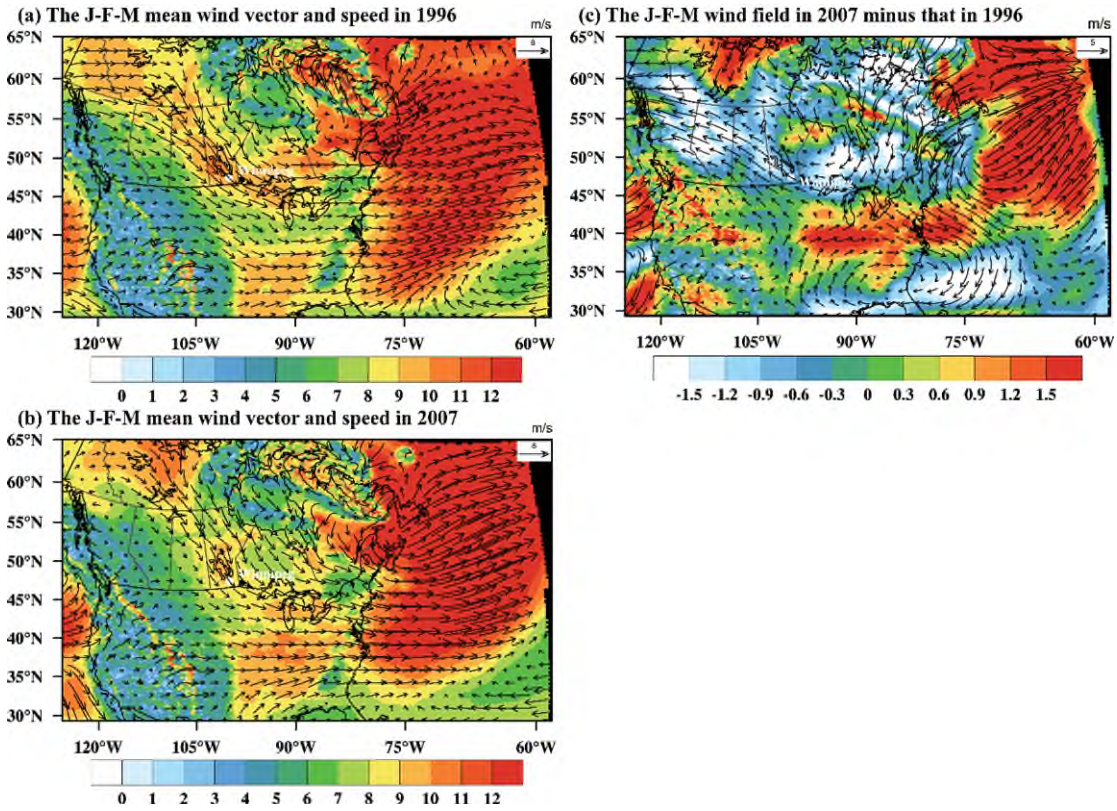

Figure S2. Same as in Figure S1a-c except for 1996 (a) and 2007 (b).

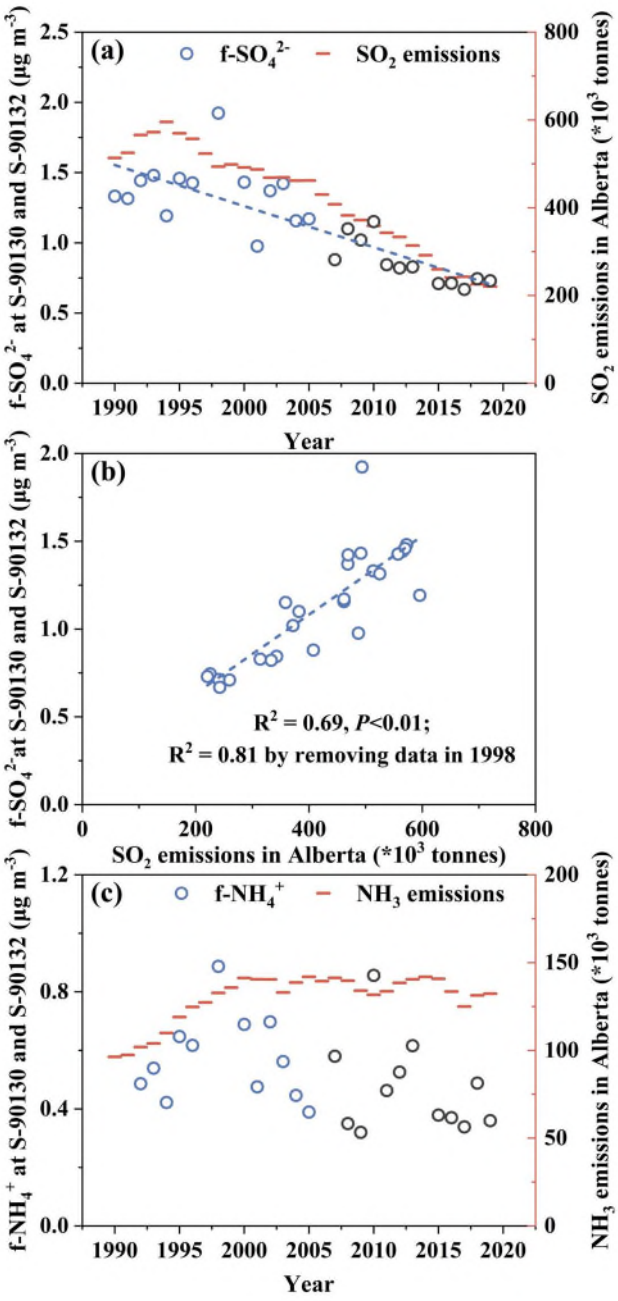

Figure S3. (a) Annual variations of mass concentrations of f-SO_4^{2-} at S-90130 and S-90132 in Edmonton and provincial total SO_2 emissions, (b) f-SO_4^{2-} vs. SO_2 emissions, and (c) same as in (a) except for f-NH_4^+ and NH_3 emissions. Blue and black markers represent the data points obtained at S-90130 and S-90132, respectively.

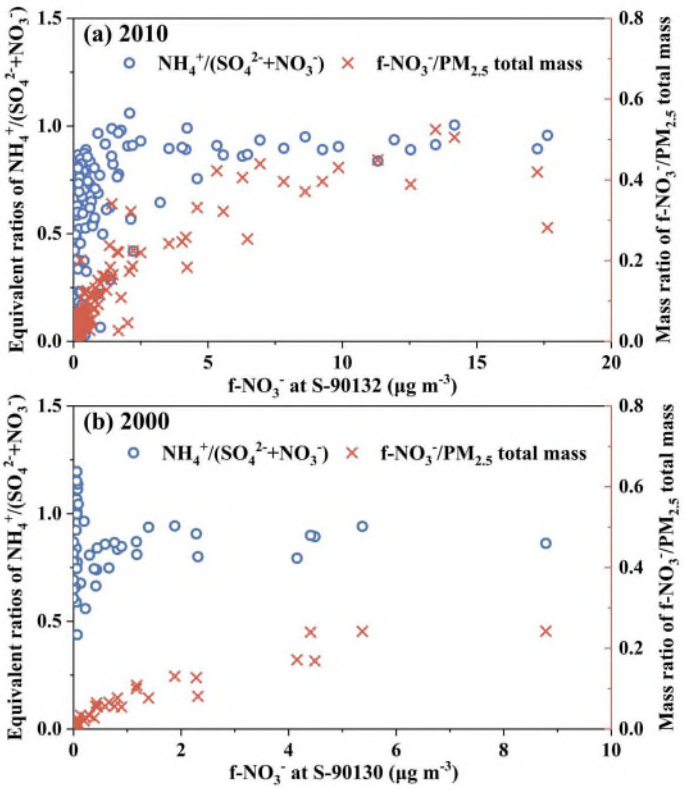

Figure S4. Variations of equivalent ratio of $NH_4^+/(SO_4^{2-}+NO_3^-)$ and mass ratio of f-$NO_3^-/PM_{2.5}$ with f-NO_3^- concentration at S-901932 in Edmonton in 2010 (a) and 2000 (b).

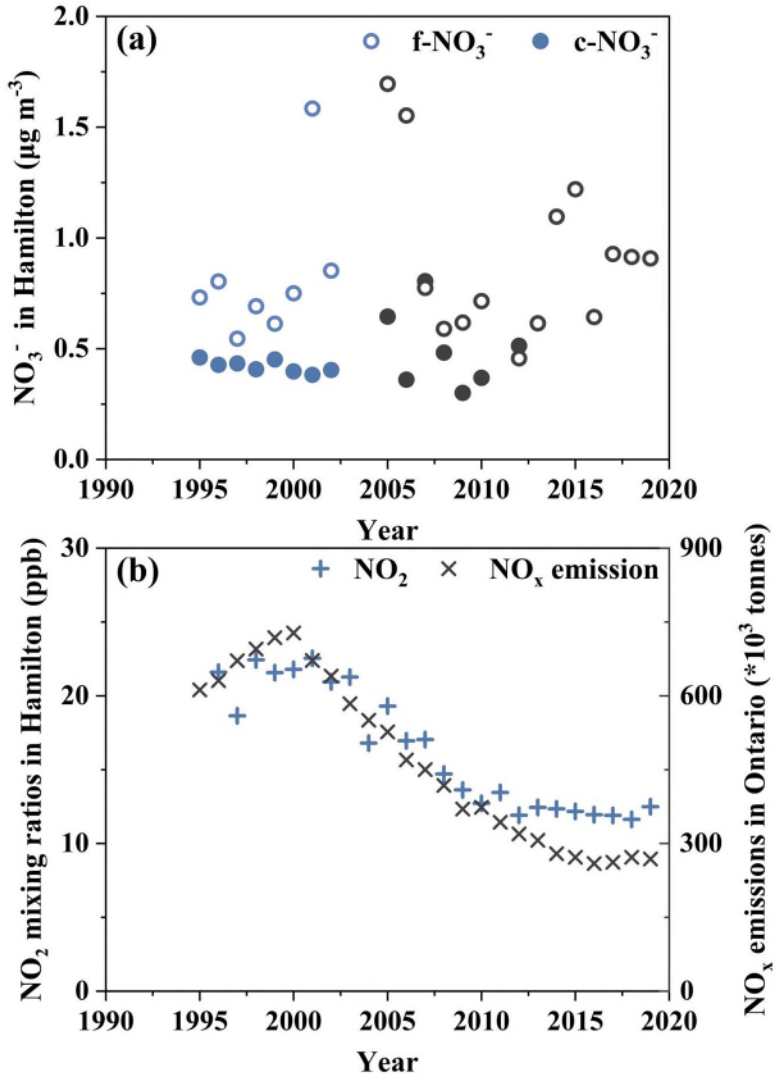

Figure S5. (a) Annual variations of mass concentrations of f-NO_3^- and c-NO_3^- in Hamilton, and (b) annual variations of mixing ratio of NO_2 in Hamilton and provincial total NO_x emissions. Blue and black markers in (a) represent data points before and after 2005, respectively.

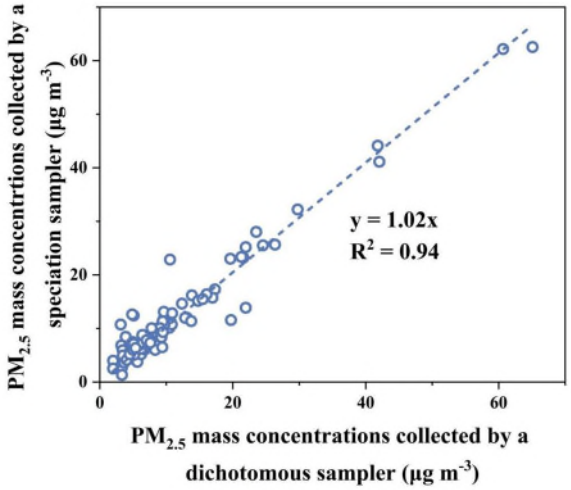

Figure S6. $PM_{2.5}$ mass concentrations measured by a speciation sampler against those measured by a dichotomous sampler at S-90132 in 2010.

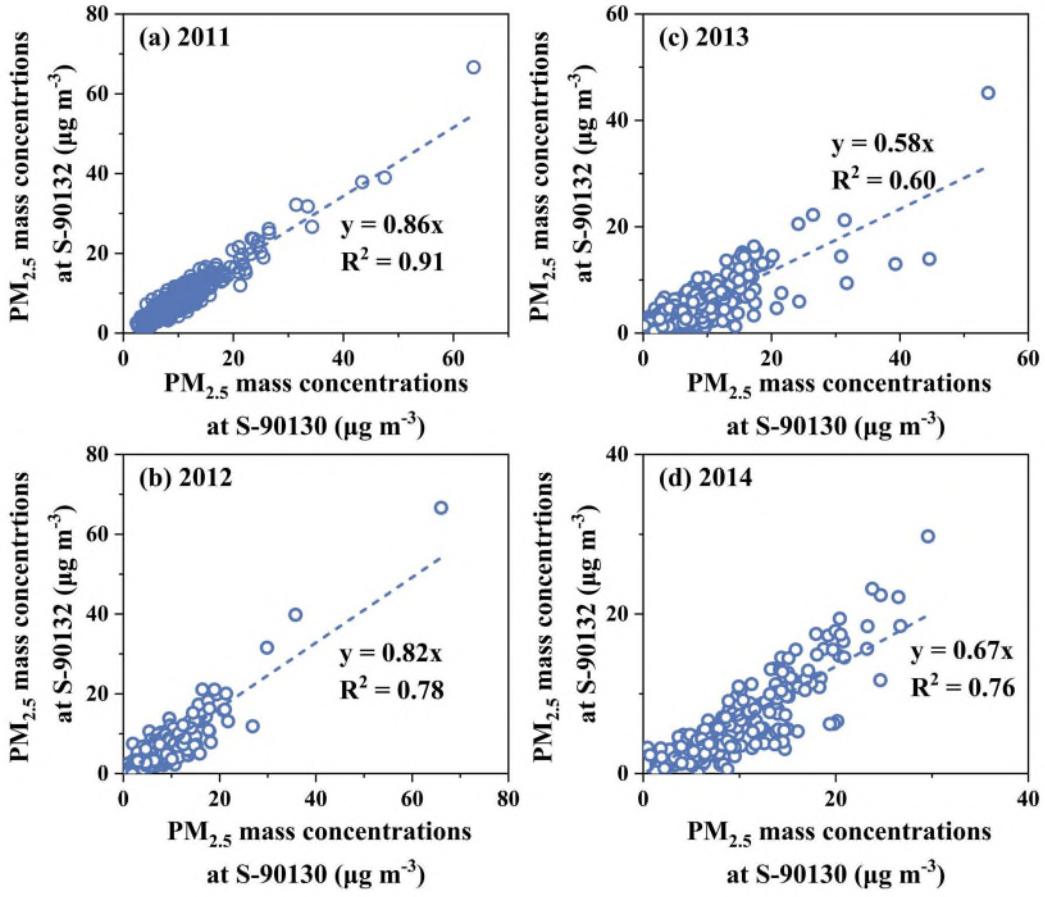

Figure S7. Inter-comparison between real-time measurements of $PM_{2.5}$ mass concentrations simultaneously made at S-90132 and S-90130 in (a) 2011, (b) 2012, (c) 2013, and (d) 2014

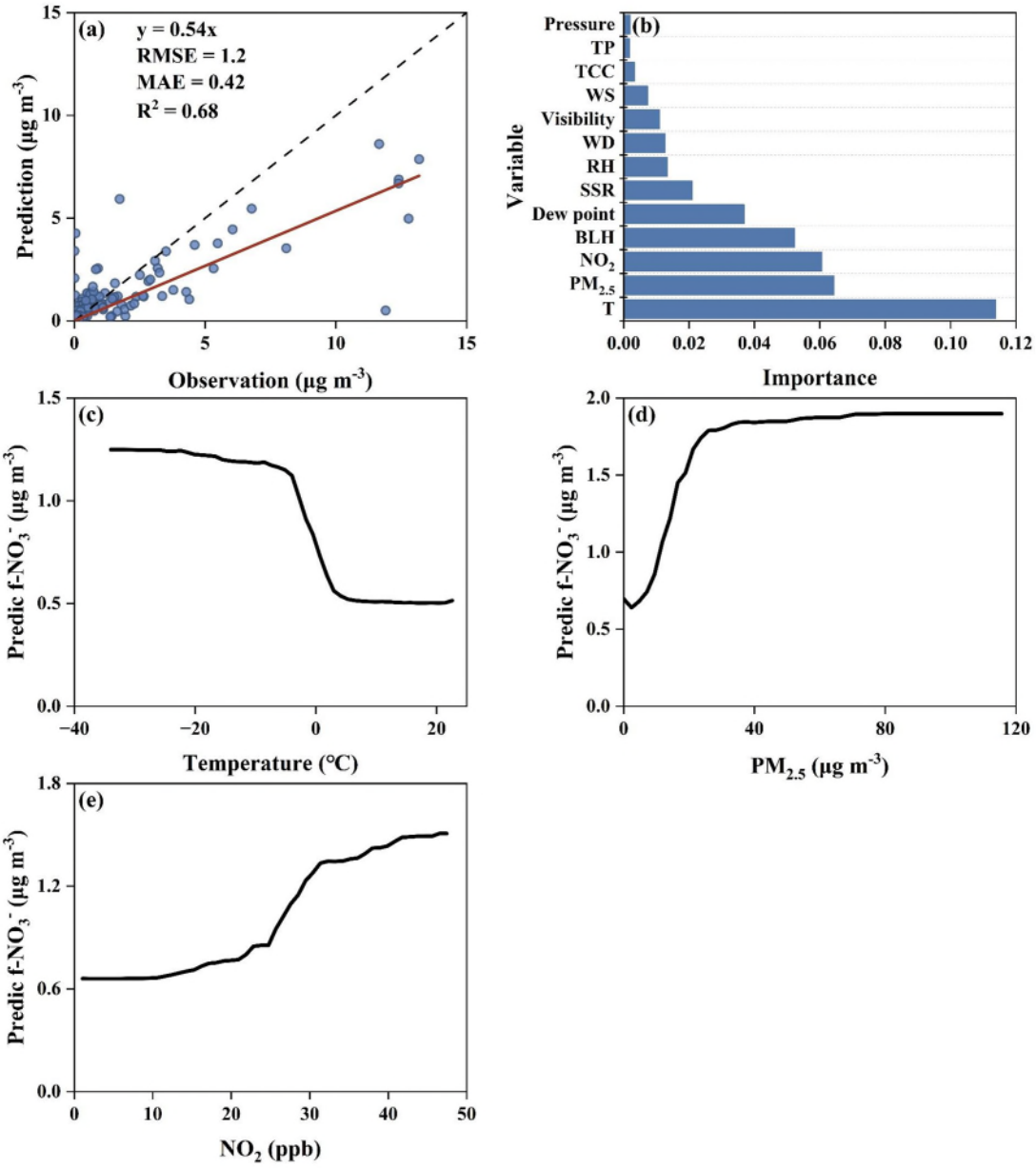

Figure S8. (a) Performance of the Random Forest model for daily f-NO_3^- during 2010–2019, shown as predicted vs. observed values for the 30% test dataset (1:1 line shown; metrics inset); (b) Permutation-based variable importance analysis diagnosing the relative influence of meteorological variables (WS, WD, RH, T, Pressure, Visibility, Dew point, BLH, SSR, TCC, and TP) and chemical species (NO_2 and $PM_{2.5}$) on f-NO_3^- formation; and Partial Dependence Plot (PDP) of Temperature (c), $PM_{2.5}$ (d) and NO_2 (e).